Vapour pressure deficit is the main driver of tree canopy conductance across biomes

Victor Flo[1,1], Jordi Martínez-Vilalta[1,1], Víctor Granda[1,1], Maurizio Mencuccini[1,1], and Rafael Poyatos[1,1]

[1]CREAF

November 30, 2022

Abstract

We aim to identify the relative importance of vapour pressure deficit (VPD), soil water content (SWC) and photosynthetic photon flux density (PPFD) as drivers of tree canopy conductance, which is a key source of uncertainty for modelling vegetation responses under climate change. We use sap flow time series of 1858 trees in 122 sites from the SAPFLUXNET global database to obtain whole-tree canopy conductance (G). The coupling, defined as the percentage of variance (R2) of G explained by the three main hydrometeorological drivers (VPD, SWC and PPFD), was evaluated using linear mixed models. For each hydrometeorological driver we assess differences in coupling among biomes, and use multiple linear regression to explain R2 by climate, soil and vegetation structure. We found that in most areas tree canopy conductance is better explained by VPD than by SWC or PPFD. We also found that sites in drylands are less coupled to all three hydrometeorological drivers than those in other biomes. Climate, soil and vegetation structure were common controls of all three hydrometeorological couplings with G, with wetter climates, fine textured soils and tall vegetation being associated to tighter coupling. Differences across sites in the hydrometeorological coupling of tree canopy conductance may affect predictions of ecosystem dynamics under future climates, and should be accounted for explicitly in models.

Vapour pressure deficit is the main driver of tree canopy conductance across biomes

Víctor Flo[1], Jordi Martínez-Vilalta[1,2], Víctor Granda[1], Maurizio Mencuccini[1,3], Rafael Poyatos[1,2]

[1]CREAF, E08193 Bellaterra (Cerdanyola del Vallès), Catalonia, Spain

[2]Univ Autònoma de Barcelona, Cerdanyola del Vallès 08193, Spain

[3]ICREA, Barcelona 08010, Spain

***Corresponding author: Víctor Flo (v.flo@creaf.uab.cat)**

VF: 0000-0003-1908-4577

JMV: 0000-0002-2332-7298

VG: 0000-0002-0469-1991

MM: 0000-0003-0840-1477

RP: 0000-0003-0521-2523

Key points

- Vapour pressure deficit is the main driver of tree canopy conductance globally.
- Tree canopy conductance dynamics are poorly explained by the main hydrometeorological drivers in drylands.
- Tree canopy conductance is more tightly couplet to hydrometeorological drivers in wetter sites, fine textured soils and tall vegetation.

Abstract

We aim to identify the relative importance of vapour pressure deficit (VPD), soil water content (SWC) and photosynthetic photon flux density (PPFD) as drivers of tree canopy conductance, which is a key source of uncertainty for modelling vegetation responses under climate change. We use sap flow time series of 1858 trees in 122 sites from the SAPFLUXNET global database to obtain whole-tree canopy conductance (*G*). The coupling, defined as the percentage of variance (R^2) of *G* explained by the three main hydrometeorological drivers (VPD, SWC and PPFD), was evaluated using linear mixed models. For each hydrometeorological driver we assess differences in coupling among biomes, and use multiple linear regression to explain R^2 by climate, soil and vegetation structure. We found that in most areas tree canopy conductance is better explained by VPD than by SWC or PPFD. We also found that sites in drylands are less coupled to all three hydrometeorological drivers than those in other biomes. Climate, soil and vegetation structure were common controls of all three hydrometeorological couplings with *G*, with wetter climates, fine textured soils and tall vegetation being associated to tighter coupling. Differences across sites in the hydrometeorological coupling of tree canopy conductance may affect predictions of ecosystem dynamics under future climates, and should be accounted for explicitly in models.

Keywords

biome, global, radiation, sap flow, soil water content, transpiration

1. Introduction

Plants regulate transpiration in response to variation in hydrometeorological conditions. However, despite decades of ecophysiological research measuring responses of leaf, plant or ecosystem evaporative fluxes to atmospheric dryness, soil moisture and radiation (Beerling, 2015), the relative importance of these drivers in determining plant controls on transpiration at the global scale is still poorly known. It is important to disentangle the biogeographical patterns of the individual dominant drivers of transpiration control, as such drivers are expected to show spatially heterogeneous dynamics with global change (Zhou *et al.*, 2019). Thus, understanding their separate roles may help improve models to anticipate climate change impacts on vegetation function and on global water and carbon cycles, and to disentangle land-atmosphere feedbacks (Massmann *et al.*, 2019).

Conductance to water vapour (*G*) derived from leaf, plant or ecosystem evaporative fluxes has been frequently used to describe the dynamic control of transpiration by plants at different organisational and temporal scales (Jarvis & McNaughton, 1986). At short timescales, this regulation is carried out via changes in stomatal aperture. Under low soil water content (SWC) or high atmospheric water demand, which is often assessed using atmospheric vapour pressure deficit (VPD), plants reduce *G* to avoid dangerous declines in water potentials preventing physiological damage and severe dehydration (Oren *et al.*, 1999). In contrast, *G* responses to light (i.e. photosynthetic photon flux density, PPFD) are linked to plant water use efficiency (WUE). Thus, plants would increase *G* with PPFD in order to optimize photosynthesis in relation to water loss (Sperry *et al.*, 2016). In addition, PPFD effects on *G* may be driven by the need to regulate leaf temperature under high radiation levels (Fauset *et al.*, 2018). These responses have been assessed in multiple, single-site studies (Jarvis, 1976; Oren *et al.*, 1999; Wang *et al.*, 2020). However, the fact that these studies frequently used different phenomenological models and model-fitting approaches complicates synthesis efforts aimed at building a common understanding of the dynamics of *G* at broad spatial scales. In addition, most previous work focused on overall *G* sensitivity (e.g. Hoshika *et al.*, 2018), not on the importance of the individual drivers (but see for instance Bretfeld *et al.*, 2018), hampering our understanding of which hydrometeorological drivers dominate *G* regulation globally.

Large-scale syntheses of the relative importance of hydrometeorological drivers regulating transpiration have been conducted using ecosystem evapotranspiration data. Novick *et al.* (2016) compared the limiting effect of SWC and VPD across vegetation types and climates, and found that limitation on ecosystem surface conductance to water vapour caused by SWC increased with climatic dryness, but that VPD was higher than SWC limitation across most mesic biomes. Similarly, Han *et al.* (2020) also reported an increased importance of SWC with increasing ecosystem aridity, but instead found that net radiation was more relevant than VPD. Conversely, Zhao *et al.* (2019) identified that, globally, ecosystem evapotranspiration was not primarily limited by hydrometeorological drivers, but by vegetation height, followed by SWC and PPFD. However, these results may not reflect the relative importance of hydrometeorological drivers on tree transpiration regulation, since partitioning transpiration from total evapotranspiration can be problematic and show substantial variability across ecosystems (Berkelhammer *et al.*, 2016). Here, we overcome the limitations of ecosystem-scale approaches by taking advantage of the first global database of plant-level transpiration from sap flow measurements (Poyatos *et al.*, 2021).

In this study, we investigate the hydrometeorological coupling of tree-level canopy conductance by quantifying the explanatory power (R^2) of individual hydrometeorological drivers of *G* (VPD, SWC, PPFD). We also estimate the total predictive ability of a model including all three drivers. We then examine how the hydrometeorological coupling of *G* differs across biomes as a function of climate, soil properties and vegetation structure. We hypothesize differences in absolute and relative *G* coupling to the hydrometeorological drivers across biomes as a result of specific environmental constraints, with tighter coupling with VPD and SWC in drier biomes with higher exposure to drought stress. We also expect that climate, soil and vegetation structure determine the coupling of *G* with VPD, SWC and PPFD, with greater coupling in sites experiencing drier conditions and marked climatic seasonality, in fine textured soils associated with lower soil water availability, and in tall stands with low leaf areas that are expected to have tighter coupling to *G* due to thinner canopy boundary layers (Peng *et al.*, 2019).

2. Methods

2.1. Sapflow and environmental data

We extracted 1858 time series of tree sap flow from the SAPFLUXNET database (Poyatos *et al.*, 2021). These time series met our requirements for data quality (see filtering section below), did not include any experimental treatment (Table S1) and corresponded to 130 species on 122 sites (Table S2). Sub-daily sap flow time series were obtained directly in sap flux density units (SFD; [cm^3 cm^{-2}_{Asw} h^{-1}]) or, when sapwood area was not available, in whole-tree sap flow units (SF; [cm^3 h^{-1}]; 24 out of 122 data-sets). In those latter cases, SF time series were converted to SFD units by dividing SF data by an estimation of tree sapwood area (Asw) using a global allometric relationship as a function of tree basal area and functional type (i.e. angiosperm vs gymnosperm) as predictors (R^2 = 0.78; n = 2262) (Fig. S1). Sub-daily SFD time series were aggregated to daytime SFD values (i.e., 6 am to 6 pm solar time). Following Flo *et al.* (2019), sap flow time series measured with non-calibrated heat dissipation sensors were corrected for bias in absolute SFD multiplying by a constant factor (1.405).

Similarly to SFD, we obtained VPD [kPa] and PPFD [μmol m^{-2} s^{-1}] time series for each site from SAPFLUXNET on-site measurements, which were subsequently averaged to daytime values. When PPFD data were not available in the datasets (12 out of 122 sites), PPFD was calculated using the mean short-wave radiation between 6 am and 6 pm extracted from the ERA5 re-analyses data base (Copernicus Climate Change Service (C3S), 2017) and then multiplying by 2.3 to transform it into PPFD. Soil water content (SWC; v/v) data were missing in 43% of the SAPFLUXNET datasets included in this study. To ensure homogeneity across sites, we used SWC from the 15-30 cm soil depth layer obtained from the ERA5-land reanalysis dataset (Copernicus Climate Change Service (C3S), 2019) at 9x9 km resolution (see database validation in Flo *et al.*, 2021).

2.2. Data filtering

In order to minimize seasonal phenological changes in leaf area, we excluded all periods between 15 days before the first daytime average temperature under 0°C and 30 days after the last day with temperatures under 0°C, during the cold season of each site (similar to Novick *et al.*, 2016). To prevent artefacts in whole-tree canopy conductance calculation (Ewers & Oren, 2000), we filtered out rainy days –days when SWC increased– and days when average daytime VPD was under 0.3 kPa (Anderegg *et al.,* 2018). We also ensured a sufficient range in hydrometeorological conditions by discarding sites with a total VPD range below 0.5 kPa or SWC range below 0.05 $m^3\ m^{-3}$, and with PPFD maximum values below 400 $\mu mol\ m^{-2}{}_{Asw}\ s^{-1}$.

2.3. *Whole-tree canopy conductance calculation*

To obtain G_s, we firstly transformed SFD units from [$cm^3\ cm^{-2}{}_{Asw}\ h^{-1}$] to [$Kg\ m^{-2}{}_{Asw}\ s^{-1}$] and then we converted it to daytime tree canopy conductance per unit of sapwood area G_{Asw} [$mol\ m^{-2}{}_{Asw}\ s^{-1}$] following Phillips & Oren (1998) and a unit transformation (eq.1).

$$G_{Asw,j,i,k} = \frac{(115.8 + 0.4236\,T_{j,i})\,SFD_{j,i,k}}{VPD_{j,i}}\,\eta\,\frac{T_0}{(T_0 + T_{j,i})}\,e^{-0.00012 h_i} \qquad (1)$$

Where $SFD_{j,i,k}$ is the sap flux density value of each site (j), day (i), and tree (k); $T_{j,i}$ [°C] is the temperature, $VPD_{j,i}$ [kPa] is the daytime vapour pressure deficit, η equals 44.6 mol m^{-3}, T_0 is 273 K, and h [m] is the altitude of each site. For two sites where h values were not available, it was extracted from The Shuttle Radar Topography Mission (Earth Resources Observation And Science (EROS) Center, 2017).

2.4. *Hydrometeorological coupling quantification*

We define hydrometeorological coupling as the coefficient of determination (R^2) of simple and multiple linear mixed models of VPD, SWC and PPFD explaining G_{Asw} at the site-tree level. High R^2 levels imply high predictive power of hydrometeorological drivers over G_{Asw}. We fitted uni-variate models for each site using G_{Asw} as response variable and the neperian logarithm of each driver as predictor (Fig. S2). Similarly, we also fitted additive, multiple regression models of site-level G_{Asw} as a function of the logarithm of all three hydrometeorological drivers (FULL model). The hierarchical structure of species and trees within sites was taken into account using linear mixed models, implemented with the *lmer* function of the 'lme4' R package (Bates *et al.,* 2015). When sites had more than one tree per species and more than one species (54 out of 122 sites), random intercept and slopes parameters were fitted for species, and random intercept parameters for trees nested into species. When models did not converge, the random structure was simplified and only the random intercept for trees was considered (33 out of 54 sites). When sites had just one species and multiple trees (67 out of 122 sites), we fitted a random intercept for trees. When a site had multiple species and just one tree per species (1 out of 122), random intercept and slopes were fitted for species.

Since we were interested in the overall coupling of all the individuals at a site, hydrometeorological coupling was set as the conditional R^2 of the models (i.e. R^2_{VPD}, R^2_{SWC}, R^2_{PPFD}, R^2_{FULL}) (Table S3), calculated with the 'MuMIn' R package (Bartoń, 2020). We fitted simple and multiple regression models instead of more sophisticated non-linear models to reduce complexity and gain generalizability across the data sets.

Three alternative sets of models were fitted to ensure consistency of the estimated R^2_{VPD}, R^2_{SWC}, R^2_{PPFD} and R^2_{FULL} values (Fig. S3). Firstly, we checked for issues related to unbalanced distributions of G_{Asw} throughout the range of VPD, SWC or PPFD. To do that, we repeated the same models as above but using binned data (binned data models). Specifically, we calculated the average of G_{Asw} measurements comprised in 0.2 kPa VPD intervals, five site-specific SWC intervals and 250 µmol m^{-2}_{Asw} s^{-1} PPFD intervals. For each summarized G_{Asw} we defined a specific VPD, SWC and PPFD value as the average of the data inside each bin. Secondly, to avoid possible artefacts due to the different sample size at each site, models were repeated by randomly sampling 10 days per tree. We implemented a bootstrapping approach with 100 repetitions and coupling values were calculated as the median of the R^2's distributions of each model (sampled data models). Finally, the third alternative implied obtaining coupling estimates by means of more flexible generalized additive models (GAM), as implemented in the bam function of the 'mgcv' R package (Wood, 2011). These GAM models were fitted using all the data available per site and specifying the same random structure as the simple linear models described above. The alternative R^2's coupling metrics obtained with the binned data, the sampled data and the gam models were all very similar to the R^2's coupling metrics from the linear models using all data (Fig. S3), and hence the latter were used in all the following analyses.

2.5. Biome classification and plot-level bioclimatic data

The estimates of G_{Asw} hydrometeorological coupling were complemented with site-level data on climate, soil properties and vegetation structure. These data were either directly obtained from the metadata associated to each SAPFLUXNET dataset or from additional data sources. We took from SAPFLUXNET the biome corresponding to each site –obtained from Whittaker diagrams using Chelsa Climate databases (Karger *et al.,* 2017) (Fig. S4)– and carried out an exhaustive quality control to reassign site biomes as indicated by SAPFLUXNET datasets contributors (Table S2). Biomes were simplified into 5 groups; drylands (DRY), woodlands (WOOD), temperate forest (TEMP), boreal forests (BOR) and tropical forests (TROP) (Table S3 and Fig. S4).

For each site, we extracted climate information from global rasters (Fig. S5). We used monthly mean precipitation, monthly maximum temperature and monthly minimum temperature rasters for the period 1979 to 2013 from the Chelsa Climate databases (Karger *et al.,* 2017), to estimate monthly potential evapotranspiration (mPET), annual potential evapotranspiration (PET) and mean annual precipitation (MAP) using the 'envirem' R package (Title & Bemmels, 2018). Then, we calculated MAP over PET (PPET) as a water availability index, and the standard deviation of the monthly differences between mean precipitation and mPET (P-PETsd) as an index of seasonality in water availability. Relevant soil parameters were obtained from in situ SAPFLUXNET data and complemented with SoilGrids 2.0 (Hengl *et al.,* 2017) when data were not available in SAPFLUXNET (Table S4). We used the proportion of sand and clay particles in the fine earth fraction [%], the total nitrogen [g kg^{-1}] and the depth to bedrock (up to 200 cm) to characterize soils. We used bedrock depth because of its ecological relevance, but results for this variable should be considered with caution due to its particularly high variability at fine spatial scales. Stand height was available in SAPFLUXNET for most sites. When this was not the case, information was completed using the average tree height of the corresponding site (again from SAPFLUXNET, 3 out of 122 sites) or when both were absent it was extracted from the Global 1 km Forest Canopy Height raster (Simard *et al.*, 2011) (3 out of 122 sites) (Table S4). When site LAI was not available from SAPFLUXNET (37 out of 122 sites), it was estimated as the average of the 95th percentile of the period 2010 to 2016 of the MCD15A3H.006 MODIS Leaf Area Index product (0.5x0.5 km grid) (Myneni, 2015), calculated using Google Earth Engine (Gorelick *et al.*, 2017) (Table S4).

2.6. Statistical Analyses

In order to test whether the hydrometeorological coupling of G_{Asw} varies across biomes, we fitted weighted regressions using the modelled R^2_{VPD}, R^2_{SWC}, R^2_{PPFD} and R^2_{FULL} as response variables and biome as explanatory variable (fixed factor). The number of tree-days with SFD measurements in each site was used as a weighting variable. Similarly, we also tested the significance of cross-biome differences between paired hydrometeorological couplings (e.g. difference between VPD and SWC coupling, $R^2_{VPD} - R^2_{SWC}$) using the same model structure.

We further explained the biogeographical patterns in the hydrometeorological coupling across sites as a function of climate, soil properties and vegetation structure. We fitted four multiple weighted regression models with R^2_{VPD}, R^2_{SWC}, R^2_{PPFD} and R^2_{FULL} as response variables and log(PPET), log(P-PETsd), soil % clay, soil total nitrogen, soil bedrock depth, stand height and LAI as bioclimatic predictors (Fig. S5). We also used the number of tree-days of each site as weighting variable. Sand percentage was not included due to a high correlation with soil % clay (r = -0.73). A stepwise model selection process based on minimising AIC was applied. We checked for normality and homoscedasticity of residuals in all models, and we also checked for multicollinearity by quantifying Variance Inflation Factors (VIF) using the 'performance' R package (Lüdecke *et al.*, 2020). These models were combined with the rasters of bioclimatic data (at a uniform resolution of 9x9 km), to predict and map global patterns of G hydrometeorological coupling to VPD, SWC and PPFD.

We also assessed the relative importance of each hydrometeorological driver by extracting the marginal partial R^2 of each hydrometeorological variable in the FULL model. These partial R^2 were calculated using 'r2beta' function of the R 'r2glmm' package (Jaeger, 2017) and relativized by the sum of the three partial R^2 (relative R^2). These relative R^2 values can be interpreted as the relative importance of each hydrometeorological variable in explaining daily variations in canopy conductance. Then, similarly as above, we fitted three multiple weighted regression models using the estimated relative R^2 as response variables and the bioclimatic variables as predictors. The resulting models were used to project the relative importance of each hydrometeorological driver globally. All statistical analyses were performed in R 4.0.5 (R Core Team, 2021).

3. Results

We found large differences in the coupling of G_{Asw} (R^2 coupling metric) to each of the individual hydrometeorological drivers globally and among biomes (Fig. 1 and Table 1). We observed that G_{Asw} was predominantly coupled to VPD across biomes, whereas coupling to SWC and PPFD was comparatively less important (Fig. 1). The difference between the coupling to VPD and to the other two drivers was significant in all cases except for SWC on woodlands and for both SWC and PPFD in boreal biomes (Table 1). The coupling to SWC was higher for TEMP and particularly WOOD biomes whereas PPFD tended to dominate in TROP biome (marginally significant effect) (Table 1). The outcomes of the linear models show a significantly higher VPD and SWC coupling for TEMP, TROP and also WOOD biomes than for the DRY biome (Table. 1). The PPFD coupling was also lowest for the DRY biome and was significantly higher for TEMP, BOR and TROP biomes; the G_{Asw} coupling to PPFD was also significantly lower in the WOOD biome compared to TEMP and TROP biomes (Table 1). The DRY biome was the one in which all three drivers collectively (FULL model) explained less variability in G_{Asw}.

In the models explaining the biogeographical patterns of G_{Asw} hydrometeorological coupling (which explained 30-52% of the variance), soil and vegetation structure variables were identified as common controls on the G_{Asw} hydrometeorological coupling (Table 2). In particular, soil clay %, and stand height were selected for all three hydrometeorological drivers (i.e. VPD, SWC and PPFD) and the FULL model, with tighter coupling always associated to fine textured soils and taller vegetation. In addition, higher soil nitrogen concentrations had a positive effect on VPD, PPFD and overall (FULL model) coupling. Log(PPET) and bedrock depth were only selected for the R^2_{SWC} and the FULL models, in which lower climatic water availability and deeper soils were associated with looser coupling (Table 2). Higher LAI was associated with lower VPD, SWC and overall (FULL model) coupling, although the effect was only significant for the FULL model. Seasonality in water availability (P-PETsd) was not included in any of the models.

When predictions of G_{Asw} coupling to each of the hydrometeorological drivers were mapped at the global scale, spatial patterns differed substantially among drivers (Fig. 2). G_{Asw} coupling to VPD was higher than ca. 50% almost everywhere except for some sub-tropical regions. The regulation of tree water fluxes at high northern latitudes (above 50° N) and in tropical regions was highly coupled to VPD, SWC and PPFD (Fig. 2). In contrast, trees living in subtropical regions tended to be less coupled (Fig. 2), consistent with the lower coupling to individual drivers in WOOD and particularly DRY biomes (Table 1). When considering the relative importance (partial R^2) of each of the three variables in driving canopy conductance (Fig. 3), temperate regions, drylands and savannas were typically coupled to VPD, many boreal areas were coupled to PPFD, and tropical regions tended to be coupled to both VPD and PPFD (Fig. 3). Although a relevant role of SWC in conjunction with VPD was identified in some regions (e.g. SW Asia, Mediterranean basin), SWC did not consistently emerge as a regionally important, dominant predictor of G_{Asw}.

4. Discussion

This study provides the first examination of the importance of VPD, SWC and PPFD as the main hydrometeorological drivers of tree canopy conductance (*G*) at the global level. All sites presented some degree of coupling to the hydrometeorological drivers considered, although there was substantial variability in the magnitude of this coupling (i.e. R^2_{VPD}, R^2_{SWC}, R^2_{PPFD}). We demonstrate that *G* is predominantly coupled to VPD in most biomes, while *G* regulation caused by SWC and PPFD is generally comparably lower.

Our results clearly identify vapour pressure deficit as the major regulator of *G* globally. This is consistent with recent reports showing that VPD limits vegetation growth at the global scale (Babst *et al.*, 2019; Yuan *et al.*, 2019), but contradicts other studies focusing on the controls of primary productivity (Jung *et al.*, 2017; Liu *et al.*, 2020) that find a global dominant role of SWC. However, caution is needed when comparing our results with these remote sensing and ecosystem-level studies, as our sample size is much smaller (and possibly spatially biased), and our approach focuses at the plant-level and uses actual transpiration data. In addition, we consider the effect of radiation availability, which has been rarely assessed in this type of studies.

We did not observe the hypothesized increase in coupling to VPD and SWC in drier biomes, although, as expected, coupling to VPD and SWC was tighter than coupling to PPFD in temperate and particularly woodland biomes. Interestingly, the importance of SWC decreased in DRY biome, even if actual sensitivity to SWC was high (Fig. S2). This result contrasts to those found at the ecosystem level, showing that drier sites present larger SWC control over evapotranspiration than wetter ones (Novick *et al.*, 2016). This opposite result between transpiration and evapotranspiration drivers importance suggests that the bare soil and the understory contribution to ecosystem surface conductance may be large (Li *et al.*, 2019) and strongly driven by SWC in DRY biome (Scott *et al.*, 2021).

The low coupling of *G* to all three hydrometeorological drivers in drylands is intriguing and may be related to the diversity of water use strategies in water limited systems, which range from drought-deciduousness to deep rooting or high hydraulic safety (e.g. Ackerly, 2004; Jacobsen *et al.*, 2007). Deep roots reaching the groundwater, for instance, could allow sufficient water supply to uncouple transpiration from hydrometeorological drivers and specifically from shallow SWC (Barbeta & Peñuelas, 2017). At the other extreme, exposure to low water potentials results in early stomatal closure (Martin-StPaul *et al.*, 2017), effectively disconnecting transpiration from hydrometeorological drivers for long periods of the year. Memory effects (Ogle *et al.*, 2015) are also likely to be more common in water-limited systems, which may result in more complex responses of transpiration to individual hydrometeorological drivers. In addition, in water-limited regions SWC can show strong seasonal interactions with VPD (Zhou *et al.*, 2019) and PPFD (Boese *et al.*, 2019) (see also Figs. S6-S8), which could produce compound drought effects that would complicate disentangling the coupling of transpiration to individual drivers. Finally, it should also be noted that we focus here on relatively tall woody vegetation, as this is the one likely to be measured with sap flow sensors (Poyatos *et al.*, 2021), and hence our analysis excludes extremely arid sites likely to be totally driven by water availability (compare the grey areas in our Fig. 3 with Fig. 1 in Running *et al*. (2004)).

Beyond general biome effects, differences in coupling among sites were explained by differences in soil, stand structure, and to a lesser extent by climate. Besides the lower coupling with SWC in areas with less climatic water availability, consistent with the results discussed in the previous paragraph, our results show the key importance of soil characteristics, particularly texture, in explaining variability in *G* coupling. Trees increase the coupling to all three hydrometeorological drivers under high clay content (finer texture). This result is to be expected since plants in fine textured soils would effectively experience lower water potentials more gradually as SWC decreases, than plants in more coarsely textured soils that will experience a threshold-like transition from high to low water potentials (Hillel, 1998). Hence, sandy soils dry rapidly and trees end up spending a large fraction of their time at very low soil water potential, reducing the coupling. In addition, our results indicate that deeper soils (higher bedrock depth) were associated to lower coupling to SWC, consistent with the notion that access to deep water may uncouple transpiration from shallow SWC (Barbeta & Peñuelas, 2017).

Vegetation height and LAI are also important drivers of vegetation transpiration coupling. VPD, SWC and PPFD limitations to *G* were typically higher in taller trees, consistent with previous studies (Boese *et al.*, 2019; Zhao *et al.*, 2019). Tree height is associated with productive areas with high resource availability, including water. In general, taller trees have higher water transport efficiencies and lower resistance to embolism (Liu *et al.*, 2019; Flo *et al.*, 2021). These traits are associated with acquisitive water use strategies and a tighter stomatal control of transpiration (Klein, 2014). A similar argument can be used to explain tighter coupling to VPD and radiation in areas with high soil nitrogen concentrations, as the latter have been related to increased stomatal conductance (Maire *et al.*, 2015) and greater degree of stomatal control under drought (Ewers *et al.*, 1999). Taller canopies are also more aerodynamically rough and, therefore, show higher VPD coupling due to higher levels of leaf surface VPD. Interestingly, once accounting for the effect of vegetation height LAI had a negative effect on transpiration coupling to VPD. We associate this result to the fact that higher LAI is related to lush canopy structures that would have a significant proportion of the leaves effectively decoupled from the atmosphere (Zhang *et al.*, 2016).

Differences in coupling among sites should also reflect different water use strategies in the corresponding communities. These differences are reflected in part in the climatic, soil, and structural differences we studied. However, independently of coupling strength, these relationships had a relatively large proportion of unexplained variance, which could be related to contrasting water use strategies coexisting in the same biomes and even in the same sites (Anderegg *et al.*, 2018; Denham *et al.*, 2021). This implies that species traits should be accounted for if we aim to understand the fine-scale distribution of *G* responses (Flo *et al.*, 2021) and predict ecosystem-level responses to environmental variation.

In conclusion, we found that VPD is the main hydrometeorological driver of tree canopy conductance globally but we also showed that VPD coupling did not increase in warmer sites, as found in ecosystem-level studies (Novick *et al.*, 2016). The role of VPD in driving transpiration regulation will likely be larger in a warmer world, given the generalised increases in projected VPD (Grossiord *et al.*, 2020). Our results indicate clear differences in hydrometeorological couplings among biomes and under different environmental contexts, which likely underlie observed differences in the dynamics of vegetation water use, tree growth and ecosystem production. Importantly, the low hydrometeorological coupling observed in drylands suggests that models simulating vegetation-atmosphere fluxes may fail in these regions unless additional processes are considered (Pan *et al.*, 2020). An explicit consideration of plant water transport (Anderegg & Venturas, 2020) and of differences in plant water use strategies (Flo *et al.*, 2021) appear essential to characterize and model the effects of VPD, SWC and PPFD on tree water use and their variability in space and time.

Acknowledgements

This work was supported by the Spanish Ministry of Education, Culture and Sports, through a doctoral grant (FPU15/03939) awarded to VF and by the Spanish Ministry of Science and Innovation through grants CGL2014-55883-JIN and RTI2018-095297-J-I00. RP also acknowledges support by an Alexander von Humboldt Fellowship for Experienced Researchers. JM-V benefited from an ICREA Academia award.

Data availability statement

The data that support the findings of this study are openly available at Flo, V. (2021). Vapour pressure deficit is the main driver of tree canopy conductance across biomes (4.0) [Data set]. Zenodo. https://doi.org/10.5281/zenodo.5517725

The code used to obtain the results of the study can be found at https://github.com/vflo/drivers_importance

5. References

Ackerly, D. (2004) Functional strategies of chaparral shrubs in relation to seasonal water deficit and disturbance. *Ecological Monographs*, **74**, 25–44.

Anderegg, W.R.L., Konings, A.G., Trugman, A.T., Yu, K., Bowling, D.R., Gabbitas, R., Karp, D.S., Pacala, S., Sperry, J.S., Sulman, B.N. & Zenes, N. (2018) Hydraulic diversity of forests regulates ecosystem resilience during drought. *Nature*, **561**, 538–541.

Anderegg, W.R.L. & Venturas, M.D. (2020) Plant hydraulics play a critical role in Earth system fluxes. *New Phytologist*, **226**, 1535–1538.

Babst, F., Bouriaud, O., Poulter, B., Trouet, V., Girardin, M.P. & Frank, D.C. (2019) Twentieth century redistribution in climatic drivers of global tree growth. *Science Advances*, **5**, eaat4313.

Barbeta, A. & Peñuelas, J. (2017) Relative contribution of groundwater to plant transpiration estimated with stable isotopes. *Scientific Reports*, **7**, 10580.

Bartoń, K. (2020) MuMIn: Multi-Model Inference. *R package version 1.43.17*.

Bates, D., Mächler, M., Bolker, B. & Walker, S. (2015) Fitting Linear Mixed-Effects Models Using **lme4**. *Journal of Statistical Software*, **67**.

Beerling, D.J. (2015) Gas valves, forests and global change: a commentary on Jarvis (1976) 'The interpretation of the variations in leaf water potential and stomatal conductance found in canopies in the field.' *Philosophical Transactions of the Royal Society B: Biological Sciences*, **370**, 20140311.

Berkelhammer, M., Noone, D.C., Wong, T.E., Burns, S.P., Knowles, J.F., Kaushik, A., Blanken, P.D. & Williams, M.W. (2016) Convergent approaches to determine an ecosystem's transpiration fraction. *Global Biogeochemical Cycles*, **30**, 933–951.

Boese, S., Jung, M., Carvalhais, N., Teuling, A.J. & Reichstein, M. (2019) Carbon–Water Flux Coupling Under Progressive Drought. *Biogeosciences*, **16**, 2557–2572.

Bretfeld, M., Ewers, B.E. & Hall, J.S. (2018) Plant water use responses along secondary forest succession during the 2015-2016 El Niño drought in Panama. *New Phytologist*, **219**, 885–899.

Copernicus Climate Change Service (C3S) (2019) C3S ERA5-Land reanalysis. *Copernicus Climate Change Service*, May 2020.

Copernicus Climate Change Service (C3S) (2017) ERA5: Fifth generation of ECMWF atmospheric reanalyses of the global climate. *Copernicus Climate Change Service Climate Data Store (CDS)*, May 2020.

Denham, S.O., Oishi, A.C., Miniat, C.F., Wood, J.D., Yi, K., Benson, M.C. & Novick, K.A. (2021) Eastern US deciduous tree species respond dissimilarly to declining soil moisture but similarly to rising evaporative demand. *Tree Physiology*, **41**, 944–959.

Earth Resources Observation And Science (EROS) Center (2017) Shuttle Radar Topography Mission (SRTM) 1 Arc-Second Global.

Ewers, B., Oren, I., Albaugh, T.J. & Dougherty, P. (1999) Carry-over effects of water and nutrient supply on water use of Pinus taeda. *Ecological Applications*, **9**, 513–525.

Ewers, B.E. & Oren, R. (2000) Analyses of assumptions and errors in the calculation of stomatal conductance from sap flux measurements. *Tree Physiology*, **20**, 579–589.

Fauset, S., Freitas, H.C., Galbraith, D.R., Sullivan, M.J.P., Aidar, M.P.M., Joly, C.A., Phillips, O.L., Vieira, S.A. & Gloor, M.U. (2018) Differences in leaf thermoregulation and water use strategies between three co-occurring Atlantic forest tree species: Leaf energy balance of Atlantic forest trees. *Plant, Cell & Environment*, **41**, 1618–1631.

Flo, V., Martínez‐Vilalta, J., Mencuccini, M., Granda, V., Anderegg, W.R.L. & Poyatos, R. (2021) Climate and functional traits jointly mediate tree water‐use strategies. *New Phytologist*, **231**, 617–630.

Flo, V., Martinez-Vilalta, J., Steppe, K., Schuldt, B. & Poyatos, R. (2019) A synthesis of bias and uncertainty in sap flow methods. *Agricultural and Forest Meteorology*, **271**, 362–374.

Gorelick, N., Hancher, M., Dixon, M., Ilyushchenko, S., Thau, D. & Moore, R. (2017) Google Earth Engine: Planetary-scale geospatial analysis for everyone. *Remote Sensing of Environment*, **202**, 18–27.

Grossiord, C., Buckley, T.N., Cernusak, L.A., Novick, K.A., Poulter, B., Siegwolf, R.T.W., Sperry, J.S. & McDowell, N.G. (2020) Plant responses to rising vapor pressure deficit. *New Phytologist*, **226**, 1550–1566.

Han, Q., Liu, Q., Wang, T., Wang, L., Di, C., Chen, X., Smettem, K. & Singh, S.K. (2020) Diagnosis of environmental controls on daily actual evapotranspiration across a global flux tower network: the roles of water and energy. *Environmental Research Letters*, **15**, 124070.

Hengl, T., Mendes de Jesus, J., Heuvelink, G.B.M., Ruiperez Gonzalez, M., Kilibarda, M., Blagotić, A., Shangguan, W., Wright, M.N., Geng, X., Bauer-Marschallinger, B., Guevara, M.A., Vargas, R., MacMillan, R.A., Batjes, N.H., Leenaars, J.G.B., Ribeiro, E., Wheeler, I., Mantel, S. & Kempen, B. (2017) SoilGrids250m: Global gridded soil information based on machine learning. *PLOS ONE*, **12**, e0169748.

Hillel, D. (1998) *Environmental soil physics*, Academic Press, San Diego, CA.

Hoshika, Y., Osada, Y., de Marco, A., Peñuelas, J. & Paoletti, E. (2018) Global diurnal and nocturnal parameters of stomatal conductance in woody plants and major crops. *Global Ecology and Biogeography*, **27**, 257–275.

Jacobsen, A.L., Pratt, R.B., Davis, S.D. & Ewers, F.W. (2007) Cavitation resistance and seasonal hydraulics differ among three arid Californian plant communities. *Plant, Cell & Environment*, **30**, 1599–1609.

Jaeger, B. (2017) r2glmm: Computes R Squared for Mixed (Multilevel) Models. *CRAN version 0.1.2.*

Jarvis, P.G. (1976) The interpretation of the variations in leaf water potential and stomatal conductance found in canopies in the field. *Philosophical Transactions of the Royal Society of London. B, Biological Sciences*, **273**, 593–610.

Jarvis, P.G. & McNaughton, K.G. (1986) *Stomatal Control of Transpiration: Scaling Up from Leaf to Region*. *Advances in Ecological Research*, pp. 1–49. Elsevier.

Jung, M., Reichstein, M., Schwalm, C.R., Huntingford, C., Sitch, S., Ahlström, A., Arneth, A., Camps-Valls, G., Ciais, P., Friedlingstein, P., Gans, F., Ichii, K., Jain, A.K., Kato, E., Papale, D., Poulter, B., Raduly, B., Rödenbeck, C., Tramontana, G., Viovy, N., Wang, Y.-P., Weber, U., Zaehle, S. & Zeng, N. (2017) Compensatory water effects link yearly global land CO2 sink changes to temperature. *Nature*, **541**, 516–520.

Karger, D.N., Conrad, O., Böhner, J., Kawohl, T., Kreft, H., Soria-Auza, R.W., Zimmermann, N.E., Linder, H.P. & Kessler, M. (2017) Climatologies at high resolution for the earth's land surface areas. *Scientific Data*, **4**, 170122.

Klein, T. (2014) The variability of stomatal sensitivity to leaf water potential across tree species indicates a continuum between isohydric and anisohydric behaviours. *Functional Ecology*, **28**, 1313–1320.

Li, X., Gentine, P., Lin, C., Zhou, S., Sun, Z., Zheng, Y., Liu, J. & Zheng, C. (2019) A simple and objective method to partition evapotranspiration into transpiration and evaporation at eddy-covariance sites. *Agricultural and Forest Meteorology*, **265**, 171–182.

Liu, H., Gleason, S.M., Hao, G., Hua, L., He, P., Goldstein, G. & Ye, Q. (2019) Hydraulic traits are coordinated with maximum plant height at the global scale. *Science Advances*, **5**, eaav1332.

Liu, L., Gudmundsson, L., Hauser, M., Qin, D., Li, S. & Seneviratne, S.I. (2020) Soil moisture dominates dryness stress on ecosystem production globally. *Nature Communications*, **11**, 4892.

Lüdecke, Makowski, Waggoner, & Patil (2020) Assessment of Regression Models Performance. *CRAN*.

Maire, V., Wright, I.J., Prentice, I.C., Batjes, N.H., Bhaskar, R., van Bodegom, P.M., Cornwell, W.K., Ellsworth, D., Niinemets, Ü., Ordonez, A., Reich, P.B. & Santiago, L.S. (2015) Global effects of soil and climate on leaf photosynthetic traits and rates: Effects of soil and climate on photosynthetic traits. *Global Ecology and Biogeography*, **24**, 706–717.

Martin-StPaul, N., Delzon, S. & Cochard, H. (2017) Plant resistance to drought depends on timely stomatal closure. *Ecology Letters*, **20**, 1437–1447.

Massmann, A., Gentine, P. & Lin, C. (2019) When Does Vapor Pressure Deficit Drive or Reduce Evapotranspiration? *Journal of Advances in Modeling Earth Systems*, **11**, 3305–3320.

Myneni, Y.K. (2015) MCD15A3H MODIS/Terra+Aqua Leaf Area Index/FPAR 4-day L4 Global 500m SIN Grid V006. *NASA EOSDIS Land Processes DAAC*, May 2020.

Novick, K.A., Ficklin, D.L., Stoy, P.C., Williams, C.A., Bohrer, G., Oishi, A.C., Papuga, S.A., Blanken, P.D., Noormets, A., Sulman, B.N., Scott, R.L., Wang, L. & Phillips, R.P. (2016) The increasing importance of atmospheric demand for ecosystem water and carbon fluxes. *Nature Climate Change*, **6**, 1023–1027.

Ogle, K., Barber, J.J., Barron-Gafford, G.A., Bentley, L.P., Young, J.M., Huxman, T.E., Loik, M.E. & Tissue, D.T. (2015) Quantifying ecological memory in plant and ecosystem processes. *Ecology Letters*, **18**, 221–235.

Oren, R., Sperry, J.S., Katul, G.G., Pataki, D.E., Ewers, B.E., Phillips, N. & Schäfer, K.V.R. (1999) Survey and synthesis of intra- and interspecific variation in stomatal sensitivity to vapour pressure deficit: Intra- and interspecific variation in stomatal sensitivity to vapour pressure deficit. *Plant, Cell & Environment*, **22**, 1515–1526.

Pan, S., Pan, N., Tian, H., Friedlingstein, P., Sitch, S., Shi, H., Arora, V.K., Haverd, V., Jain, A.K., Kato, E., Lienert, S., Lombardozzi, D., Nabel, J.E.M.S., Ottlé, C., Poulter, B., Zaehle, S. &

Running, S.W. (2020) Evaluation of global terrestrial evapotranspiration using state-of-the-art approaches in remote sensing, machine learning and land surface modeling. *Hydrology and Earth System Sciences*, **24**, 1485–1509.

Peng, L., Zeng, Z., Wei, Z., Chen, A., Wood, E.F. & Sheffield, J. (2019) Determinants of the ratio of actual to potential evapotranspiration. *Global Change Biology*, **25**, 1326–1343.

Phillips, N. & Oren, R. (1998) A comparison of daily representations of canopy conductance based on two conditional time-averaging methods and the dependence of daily conductance on environmental factors. *Annales des Sciences Forestières*, **55**, 217–235.

Poyatos, R., Granda, V., Flo, V., Adams, M.A., Adorján, B., Aguadé, D., Aidar, M.P.M., Allen, S., Alvarado-Barrientos, M.S., Anderson-Teixeira, K.J., Aparecido, L.M., Arain, M.A., Aranda, I., Asbjornsen, H., Baxter, R., Beamesderfer, E., Berry, Z.C., Berveiller, D., Blakely, B., Boggs, J., Bohrer, G., Bolstad, P.V., Bonal, D., Bracho, R., Brito, P., Brodeur, J., Casanoves, F., Chave, J., Chen, H., Cisneros, C., Clark, K., Cremonese, E., Dang, H., David, J.S., David, T.S., Delpierre, N., Desai, A.R., Do, F.C., Dohnal, M., Domec, J.-C., Dzikiti, S., Edgar, C., Eichstaedt, R., El-Madany, T.S., Elbers, J., Eller, C.B., Euskirchen, E.S., Ewers, B., Fonti, P., Forner, A., Forrester, D.I., Freitas, H.C., Galvagno, M., Garcia-Tejera, O., Ghimire, C.P., Gimeno, T.E., Grace, J., Granier, A., Griebel, A., Guangyu, Y., Gush, M.B., Hanson, P.J., Hasselquist, N.J., Heinrich, I., Hernandez-Santana, V., Herrmann, V., Hölttä, T., Holwerda, F., Irvine, J., Isarangkool Na Ayutthaya, S., Jarvis, P.G., Jochheim, H., Joly, C.A., Kaplick, J., Kim, H.S., Klemedtsson, L., Kropp, H., Lagergren, F., Lane, P., Lang, P., Lapenas, A., Lechuga, V., Lee, M., Leuschner, C., Limousin, J.-M., Linares, J.C., Linderson, M.-L., Lindroth, A., Llorens, P., López-Bernal, Á., Loranty, M.M., Lüttschwager, D., Macinnis-Ng, C., Maréchaux, I., Martin, T.A., Matheny, A., McDowell, N., McMahon, S., Meir, P., Mészáros, I., Migliavacca, M., Mitchell, P., Mölder, M., Montagnani, L., Moore, G.W., Nakada, R., Niu, F., Nolan, R.H., Norby, R., Novick, K., Oberhuber, W., Obojes, N., Oishi, A.C., Oliveira, R.S., Oren, R., Ourcival, J.-M., Paljakka, T., Perez-Priego, O., Peri, P.L., Peters, R.L., Pfautsch, S., Pockman, W.T., Preisler, Y., Rascher, K., Robinson, G., Rocha, H., Rocheteau, A., Röll, A., Rosado, B.H.P., Rowland, L., Rubtsov, A.V., Sabaté, S., Salmon, Y., Salomón, R.L., Sánchez-Costa, E., Schäfer, K.V.R., Schuldt, B., Shashkin, A., Stahl, C., Stojanović, M., Suárez, J.C., Sun, G., Szatniewska, J., Tatarinov, F., Tesař, M., Thomas, F.M., Tor-ngern, P., Urban, J., Valladares, F., van der Tol, C., van Meerveld, I., Varlagin, A., Voigt, H., Warren, J., Werner, C., Werner, W., Wieser, G., Wingate, L., Wullschleger, S., Yi, K., Zweifel, R., Steppe, K., Mencuccini, M. & Martínez-Vilalta, J. (2021) Global transpiration data from sap flow measurements: the SAPFLUXNET database. *Earth System Science Data*, **13**, 2607–2649.

R Core Team (2021) *R: A Language and Environment for Statistical Computing*, R Foundation for Statistical Computing, Vienna, Austria.

Running, S.W., Nemani, R.R., Heinsch, F.A., Zhao, M., Reeves, M. & Hashimoto, H. (2004) A Continuous Satellite-Derived Measure of Global Terrestrial Primary Production. *BioScience*, **54**, 547–560.

Schöley, J. & Kashnitsky, I. (2020) tricolore: A Flexible Color Scale for Ternary Compositions.

Scott, R.L., Knowles, J.F., Nelson, J.A., Gentine, P., Li, X., Barron-Gafford, G., Bryant, R. & Biederman, J.A. (2021) Water Availability Impacts on Evapotranspiration Partitioning. *Agricultural and Forest Meteorology*, **297**, 108251.

Simard, M., Pinto, N., Fisher, J.B. & Baccini, A. (2011) Mapping forest canopy height globally with spaceborne lidar. *Journal of Geophysical Research*, **116**, G04021.

Sperry, J.S., Wang, Y., Wolfe, B.T., Mackay, D.S., Anderegg, W.R.L., McDowell, N.G. & Pockman, W.T. (2016) Pragmatic hydraulic theory predicts stomatal responses to climatic water deficits. *New Phytologist*, **212**, 577–589.

Title, P.O. & Bemmels, J.B. (2018) ENVIREM: an expanded set of bioclimatic and topographic variables increases flexibility and improves performance of ecological niche modeling. *Ecography*, **41**, 291–307.

Wang, Y., Sperry, J.S., Anderegg, W.R.L., Venturas, M.D. & Trugman, A.T. (2020) A theoretical and empirical assessment of stomatal optimization modeling. *New Phytologist*, **227**, 311–325.

Wood, S.N. (2011) Fast stable restricted maximum likelihood and marginal likelihood estimation of semiparametric generalized linear models: Estimation of Semiparametric Generalized Linear Models. *Journal of the Royal Statistical Society: Series B (Statistical Methodology)*, **73**, 3–36.

Yuan, W., Zheng, Y., Piao, S., Ciais, P., Lombardozzi, D., Wang, Y., Ryu, Y., Chen, G., Dong, W., Hu, Z., Jain, A.K., Jiang, C., Kato, E., Li, S., Lienert, S., Liu, S., Nabel, J.E.M.S., Qin, Z., Quine, T., Sitch, S., Smith, W.K., Wang, F., Wu, C., Xiao, Z. & Yang, S. (2019) Increased atmospheric vapor pressure deficit reduces global vegetation growth. *Science Advances*, **5**, eaax1396.

Zhang, Z.Z., Zhao, P., McCarthy, H.R., Zhao, X.H., Niu, J.F., Zhu, L.W., Ni, G.Y., Ouyang, L. & Huang, Y.Q. (2016) Influence of the decoupling degree on the estimation of canopy stomatal conductance for two broadleaf tree species. *Agricultural and Forest Meteorology*, **221**, 230–241.

Zhao, W.L., Gentine, P., Reichstein, M., Zhang, Y., Zhou, S., Wen, Y., Lin, C., Li, X. & Qiu, G.Y. (2019) Physics‐Constrained Machine Learning of Evapotranspiration. *Geophysical Research Letters*, **46**, 14496–14507.

Zhou, S., Williams, A.P., Berg, A.M., Cook, B.I., Zhang, Y., Hagemann, S., Lorenz, R., Seneviratne, S.I. & Gentine, P. (2019) Land–atmosphere feedbacks exacerbate concurrent soil drought and atmospheric aridity. *Proceedings of the National Academy of Sciences*, **116**, 18848–18853.

Table 1. Analysis of variance testing differences among biomes in the coupling (conditional R^2's from mixed models) of tree-level water conductance (G_{Asw}) to each of the main hydrometeorological drivers: vapour pressure deficit (R^2_{VPD}), soil water content (R^2_{SWC}), radiation (R^2_{PPFD}) and the complete model including all drivers (R^2_{FULL}). The table shows the mean coupling obtained across all sites in each biome. We also show the means of the paired differences between individual hydrometeorological couplings and the corresponding statistical significance. DRY: dry and desert biomes; WOOD: woodlands and shrublands; TEMP: temperate biomes; BOR: boreal and tundra; TROP: tropical and subtropical biomes. Different superscript letters indicate significant ($p < 0.05$) Tukey tests of paired differences between biomes. Asterisks indicate statistically significant differences from zero for the paired differences between hydrometeorological couplings.

Biome	R^2_{VPD}	R^2_{SWC}	R^2_{PPFD}	R^2_{FULL}	R^2_{VPD} - R^2_{SWC}	R^2_{VPD} - R^2_{PPFD}	R^2_{SWC} - R^2_{PPFD}	Number of sites
DRY	0.31 A	0.183 A	0.189 A	0.389 A	0.127*** BC	0.121*** AB	-0.006 A	7
WOOD	0.436 B	0.412 B	0.281 AB	0.619 B	0.024 A	0.155*** B	0.131*** B	29
TEMP	0.461 B	0.389 B	0.358 C	0.544 B	0.072*** AB	0.103*** A	0.031* A	70
BOR	0.575 ABC	0.45 AB	0.481 BC	0.603 AB	0.124 ABC	0.093 AB	-0.031 AB	8
TROP	0.601 C	0.4 B	0.457 C	0.627 B	0.201*** C	0.144*** AB	-0.057. A	8

Statistical significant levels: "." p<0.1 ; "*" p<0.05; "**" p<0.01; "***" p<0.001

Table 2. Parameters of the models explaining G_{Asw} coupling to VPD, SWC, PPFD and to all three hydrometeorological drivers (R^2_{VPD}, R^2_{SWC}, R^2_{PPFD} and R^2_{FULL}, respectively) as a function of climatic, soil and stand structure variables. log(PPET): logarithm of precipitation over potential evapotranspiration [% log(mm $mm^{-1})^{-1}$]; log(P-PETsd): logarithm of the standard deviation of the difference between precipitation and potential evapotranspiration [% log(mm)$^{-1}$]; Clay percentage [% $\%^{-1}$clay]; Total Nitrogen [% (Kg $g^{-1})^{-1}$]; Bedrock depth [% cm^{-1}]; Stand Height [% m^{-1}]; LAI: leaf area index [% $(m^2\ m^{-2})^{-1}$]. NI means that the variable was not included in the model after model selection. The R^2 of each multiple regression is also shown.

		Climate		Soil			Vegetation structure		
Variable	Intercept [%]	log(PPET)	log(P-PETsd)	Clay	Total Nitrogen	Bedrock depth	Stand Height	LAI	R^2
R^2_{VPD}	25.927 ***	NI	NI	0.314 ***	3.522 ***	NA	0.746 ***	-1.524 .	0.297
R^2_{SWC}	61.591 ***	11.692 ***	NI	0.475 ***	NI	-0.174 *	0.429 ***	-1.206 ns	0.521
R^2_{PPFD}	10.741 ***	NI	NI	0.230**	2.873 ***	NI	0.762 ***	NI	0.365
R^2_{FULL}	80.342 ***	5.932 *	NI	0.470***	1.849 *	-0.198 *	0.595 ***	-1.961 *	0.351

Statistical significant levels: "." $p<0.1$; "*" $p<0.05$; "**" $p<0.01$; "***" $p<0.001$; ns not significant.

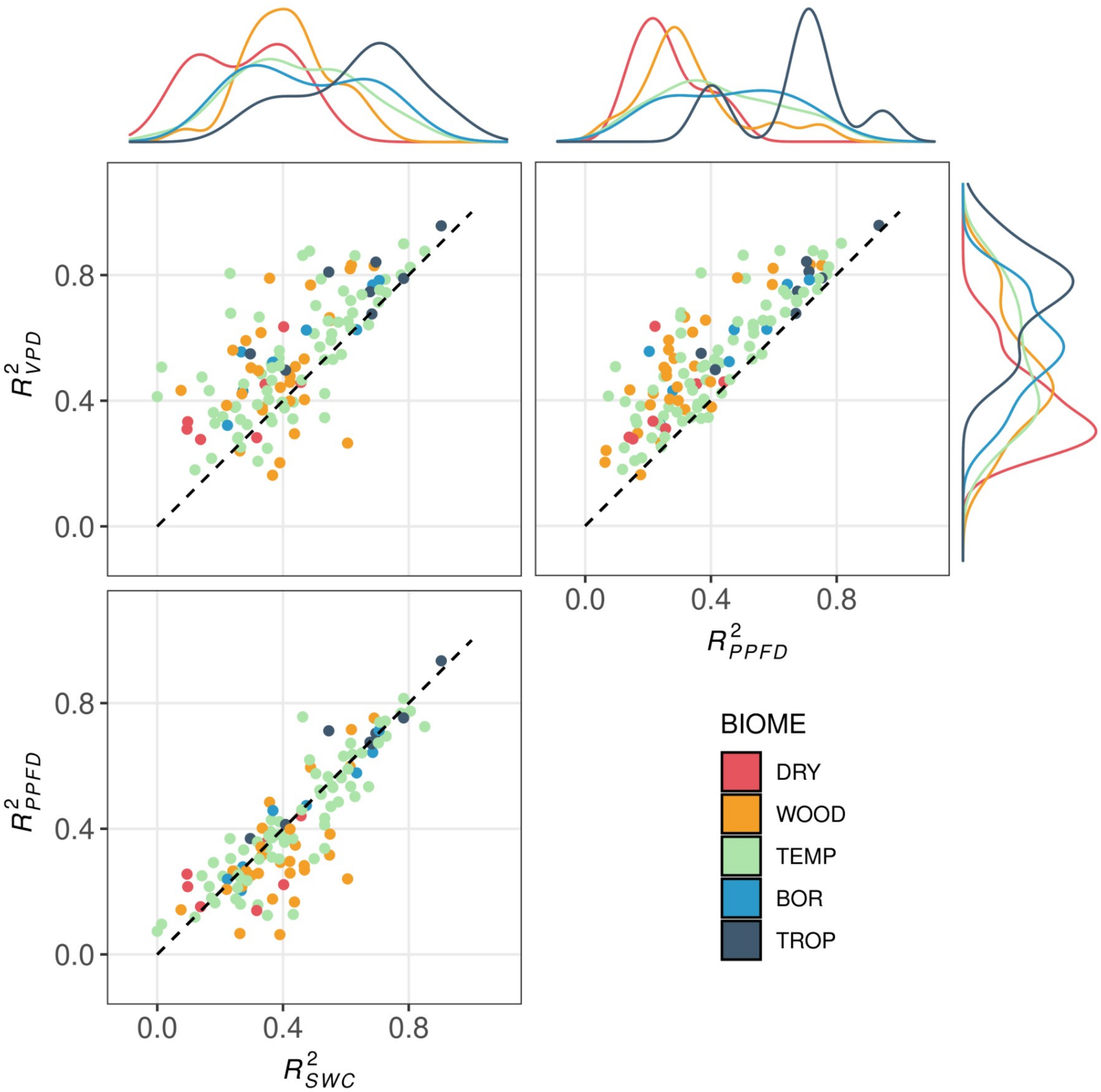

Figure 1. Bi-variate and uni-variate distributions of the coupling of G_{Asw} to the hydrometeorological drivers studied: vapour pressure deficit (R^2_{VPD}), soil water content (R^2_{SWC}) and radiation (R^2_{PPFD}) for different biomes. Points correspond to site-level modelled conditional R^2 values. Colours represent different biomes, DRY: dry and desert biomes; WOOD: woodlands and shrublands; TEMP: temperate biomes; BOR: boreal and tundra; TROP: tropical and subtropical biomes. Dashed black line shows 1:1 relation.

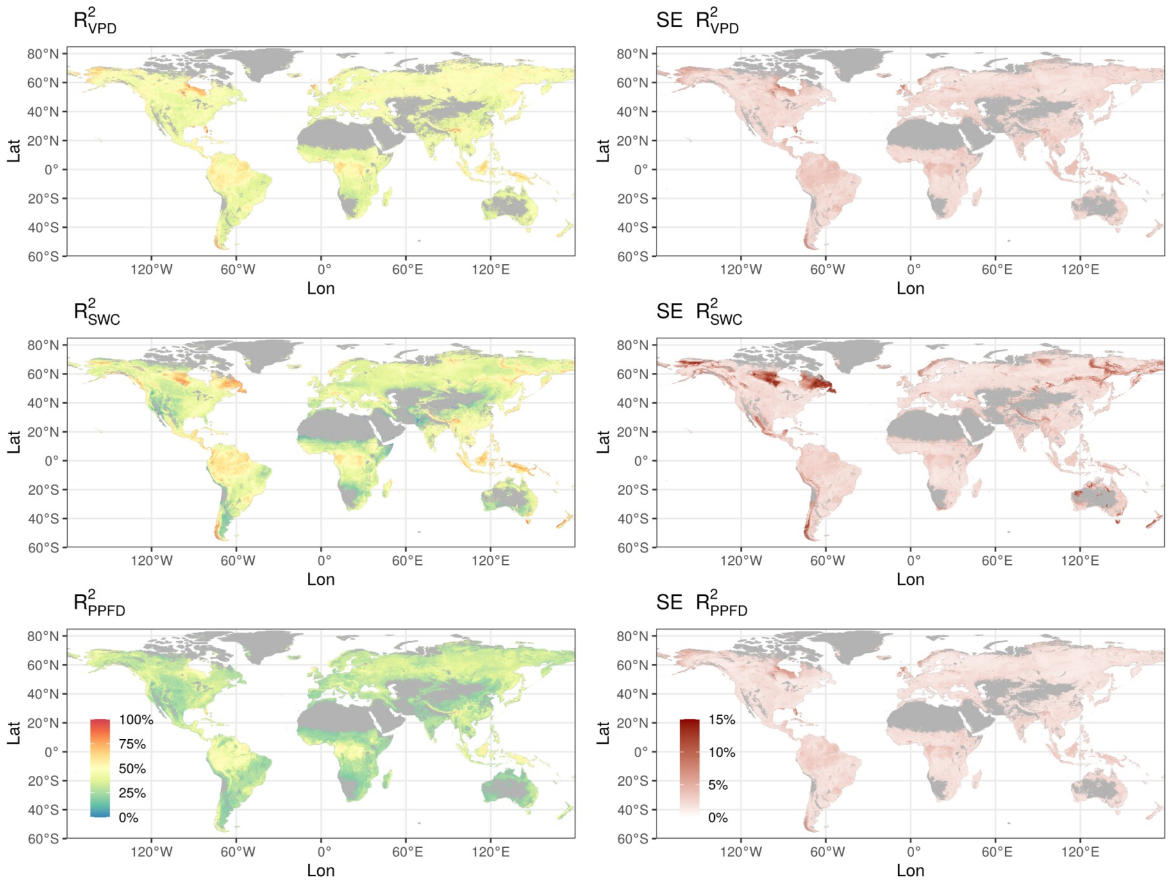

Figure 2. Global projection of G_{Asw} coupling to VPD, SWC and PPFD (R^2_{VPD}, R^2_{SWC} and R^2_{PPFD}, respectively), obtained from regression models of each coupling as a function of climatic, soil and stand structure variables (left panels). Right panels show projected Standard Error of the corresponding model.

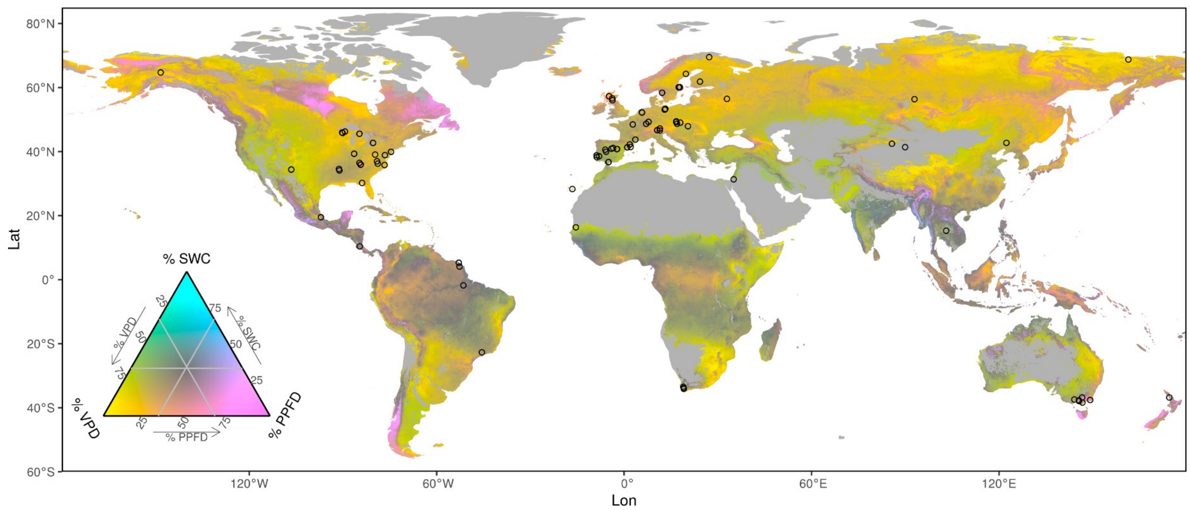

Figure 3. Relative importance (partial R^2) of the three hydrometeorological drivers of transpiration regulation calculated from the complete (FULL) model, and projected at the global scale using linear models with climate, soil and vegetation structural variables as explanatory variables. Grid values were calculated using the 'tricolore' package (Schöley & Kashnitsky, 2020) for each cell as the relative value of the projections of the relative importance of each hydrometeorological variable. Colour gradient indicate the relative importance of the three hydrometeorological constraints. Light grey colour are deserts or non-forested areas. % VPD: vapour pressure deficit relative importance. % SWC: soil water content relative importance. % PPFD: photosynthetic photon flux density relative importance. Points indicate locations of study sites.

Global Biogeochemical Cycles

Supporting Information for

Vapour pressure deficit is the main driver of tree canopy conductance across biomes

Víctor Flo[1], Jordi Martínez-Vilalta[1,2], Víctor Granda[1], Maurizio Mencuccini[1,3], Rafael Poyatos[1,2]

[1]CREAF, E08193 Bellaterra (Cerdanyola del Vallès), Catalonia, Spain

[2]Univ Autònoma de Barcelona, Cerdanyola del Vallès 08193, Spain

[3]ICREA, Barcelona 08010, Spain

Contents of this file

Figures S1 to S8

Tables S1 to S4

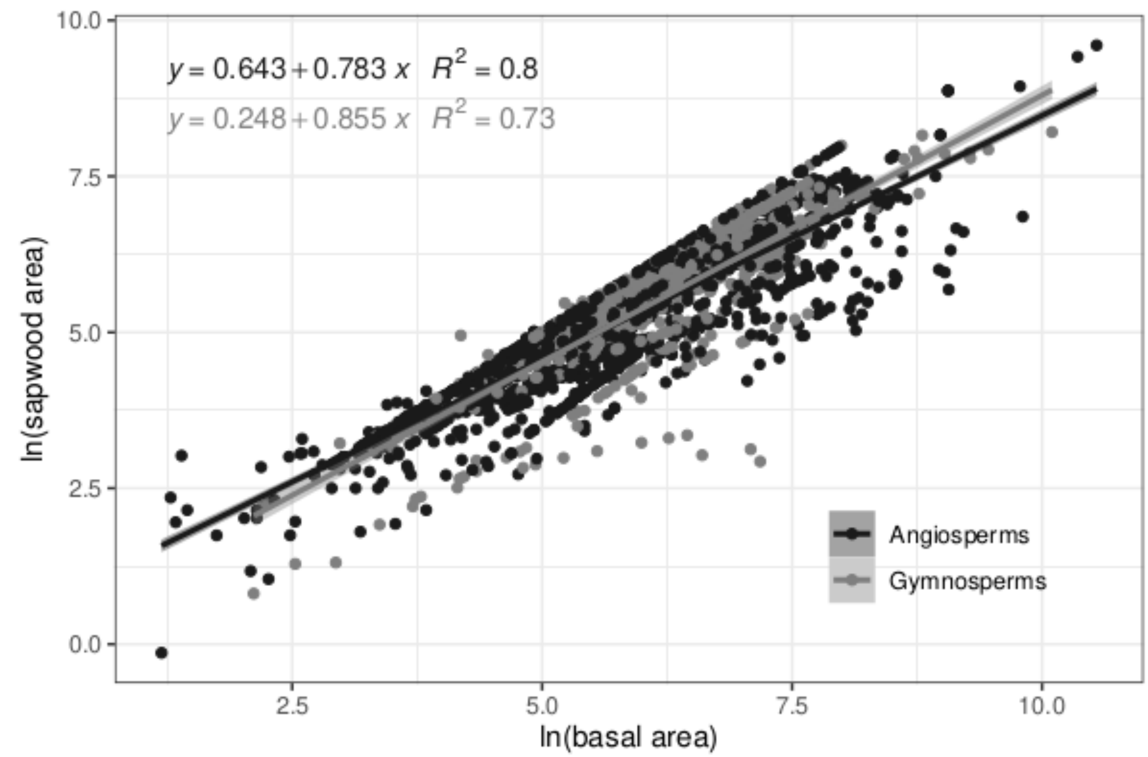

Figure S1: SAPFLUXNET global scaling relationship between basal area and sapwood area. Basal area and sapwood area are both in cm^2. Shaded areas are 95% model confidence interval.

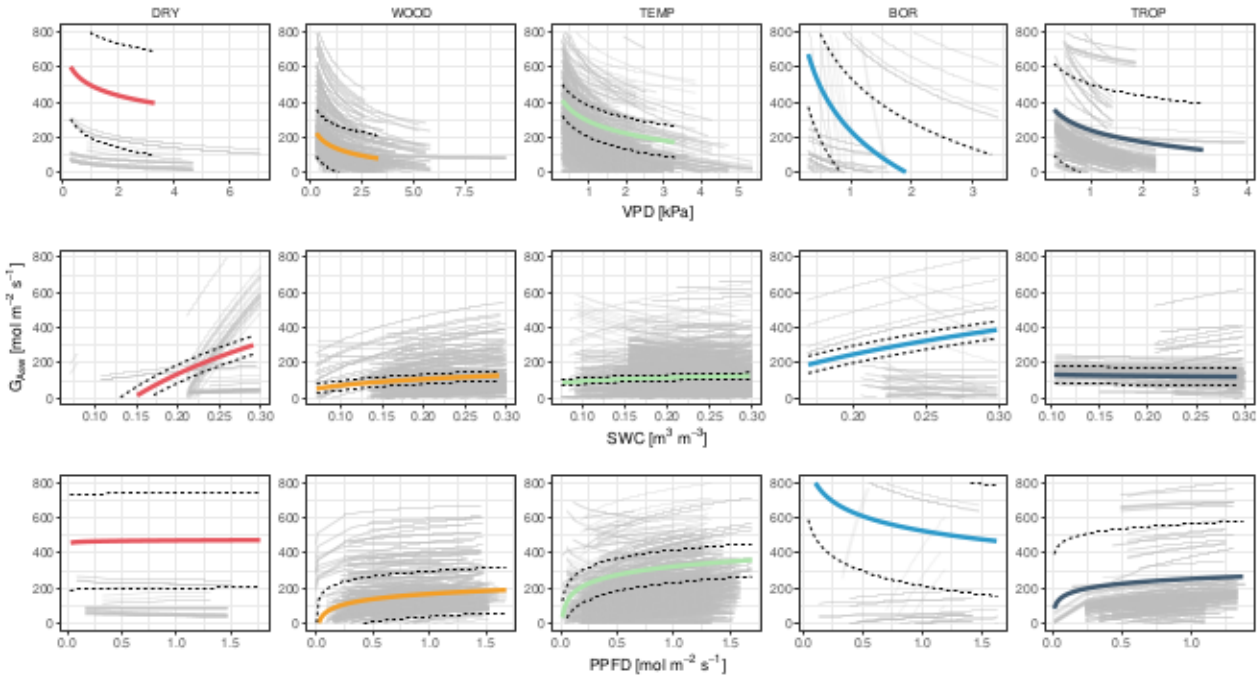

Figure S2: Log relationships of the three environmental variables estimated with the FULL model (VPD + SWC + PPFD) and grouped by biome. Coloured lines are biome-averaged models calculated from LMM predictions with G_{Asw} as response variable and the neperian logarithm of the environmental constrains as explanatory variables. Dashed line shows standard error of the average models calculated with bootstrap prediction using 100 simulations.

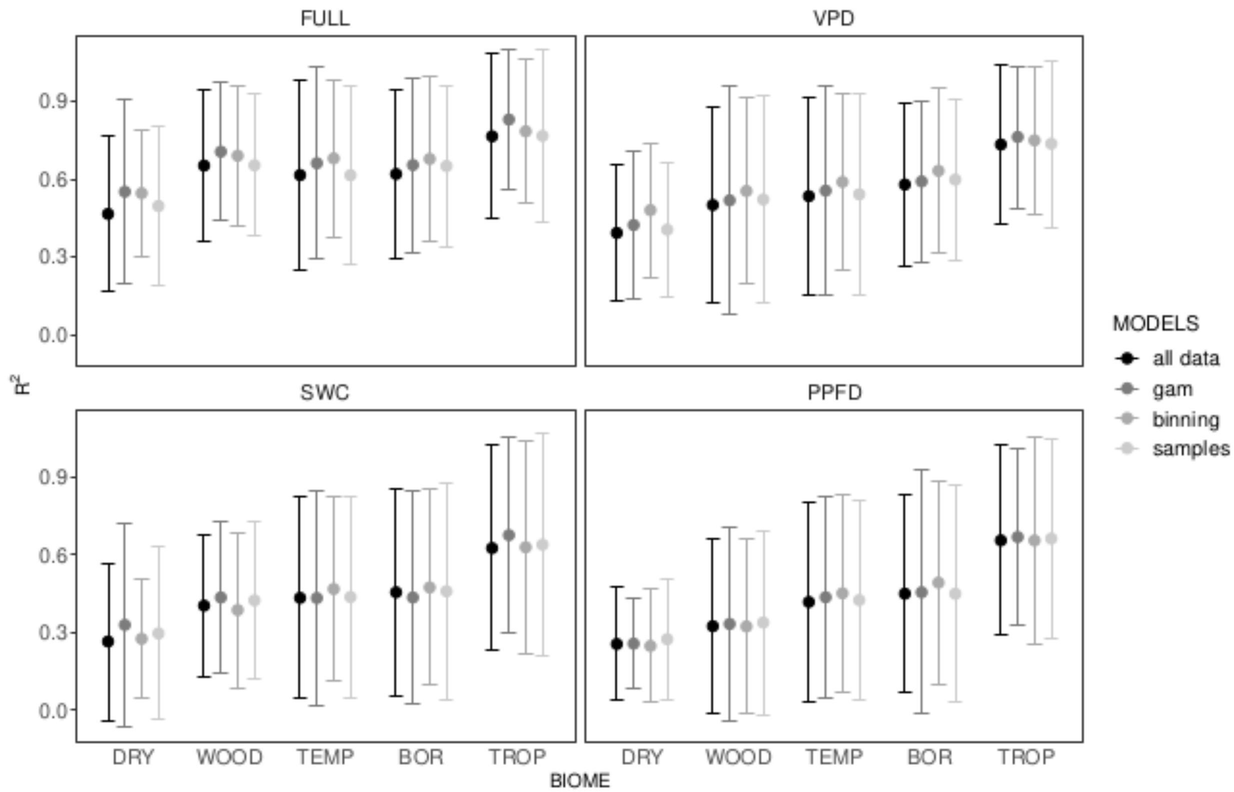

Figure S3: Comparison of biomes R^2_{FULL} (VPD + SWC + PPFD), R^2_{VPD} (VPD), R^2_{SWC} (SWC) and R^2_{PPFD} (PPFD) calculated with the four modelling approaches: using linear mixed models on all data, binned data and sampled data and, using GAM models on all data. Dots are mean values for each biome and error bars represent two standard deviations. There were no intra-biome significant differences among models.

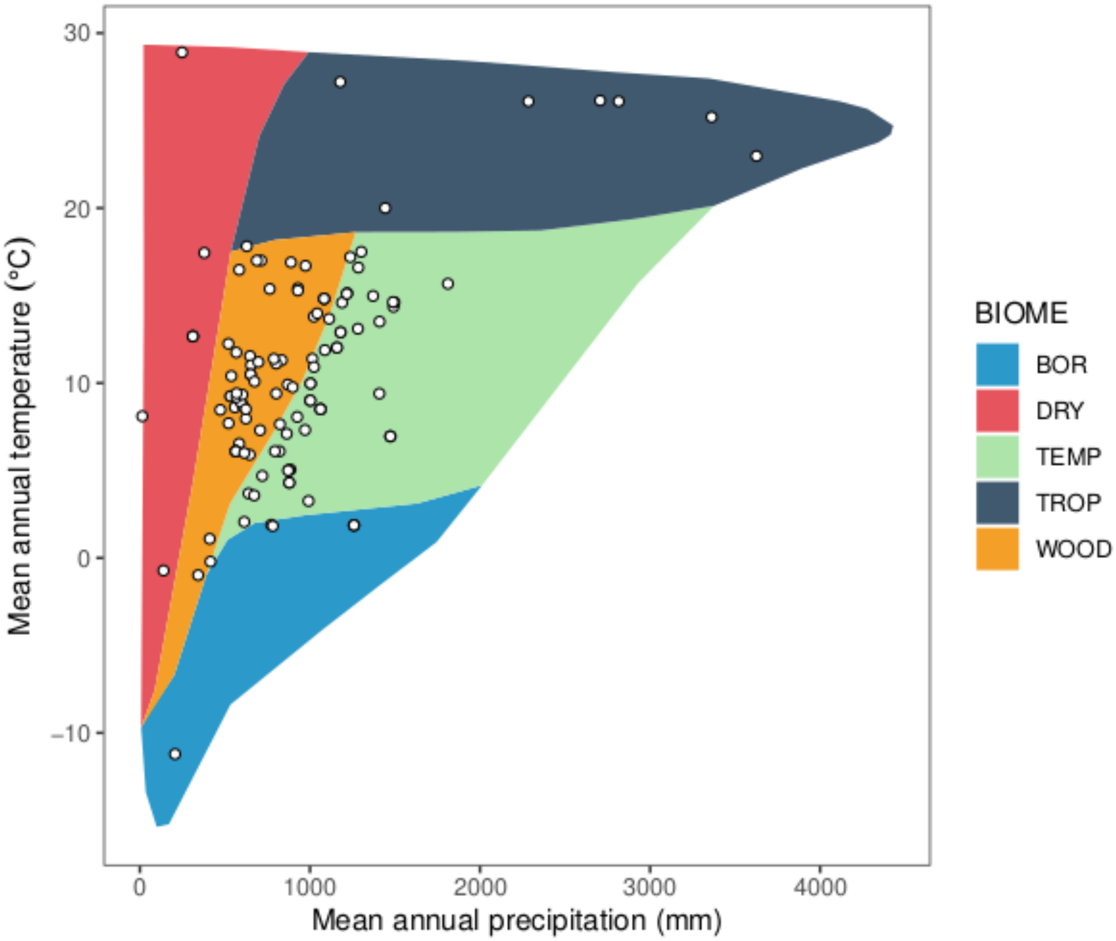

Figure S4: Bioclimatic distribution of the SAPFLUXNET datasets used in the study. Points show the different datasets in a Whittaker diagram showing the classification of the aggregated biomes used in the study.

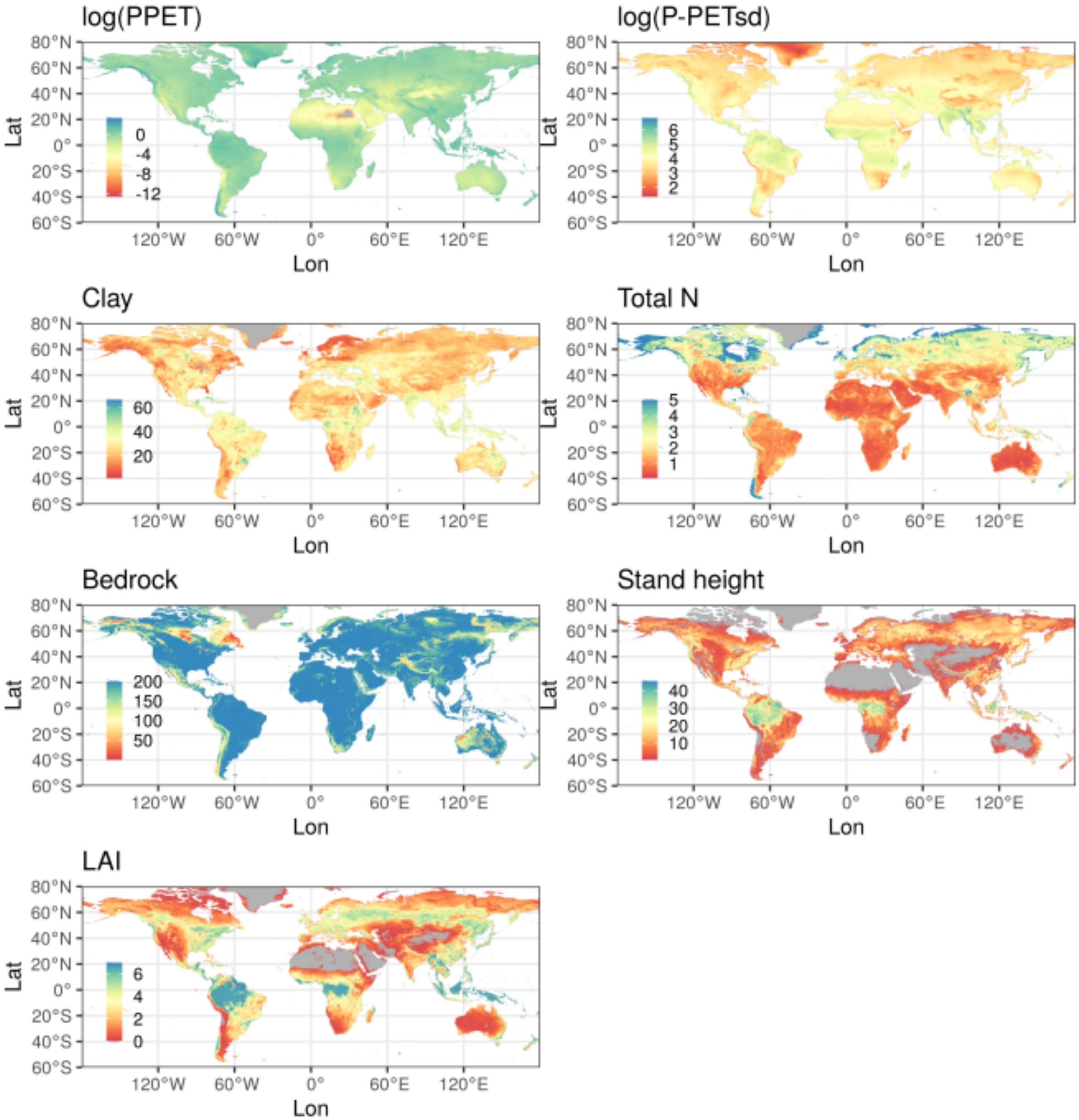

Figure S5: Global projection of climatic, soil and stand structure variables. log(PPET): logarithm of precipitation over potential evapotraspiration [log(mm mm^{-1})]; log(P-PET$_{sd}$): logarithm of the standard deviation of the difference between precipitation and potential evapotranspiration [log(mm)]; Clay: percentage of clay in the soil; Total N: total nitrogen in the soil [g kg^{-1}]; Bedrock [cm]; Stand height [m]; LAI: leaf area index [m^2 m^{-2}]. Total N values above 5 g kg^{-1} were truncated.

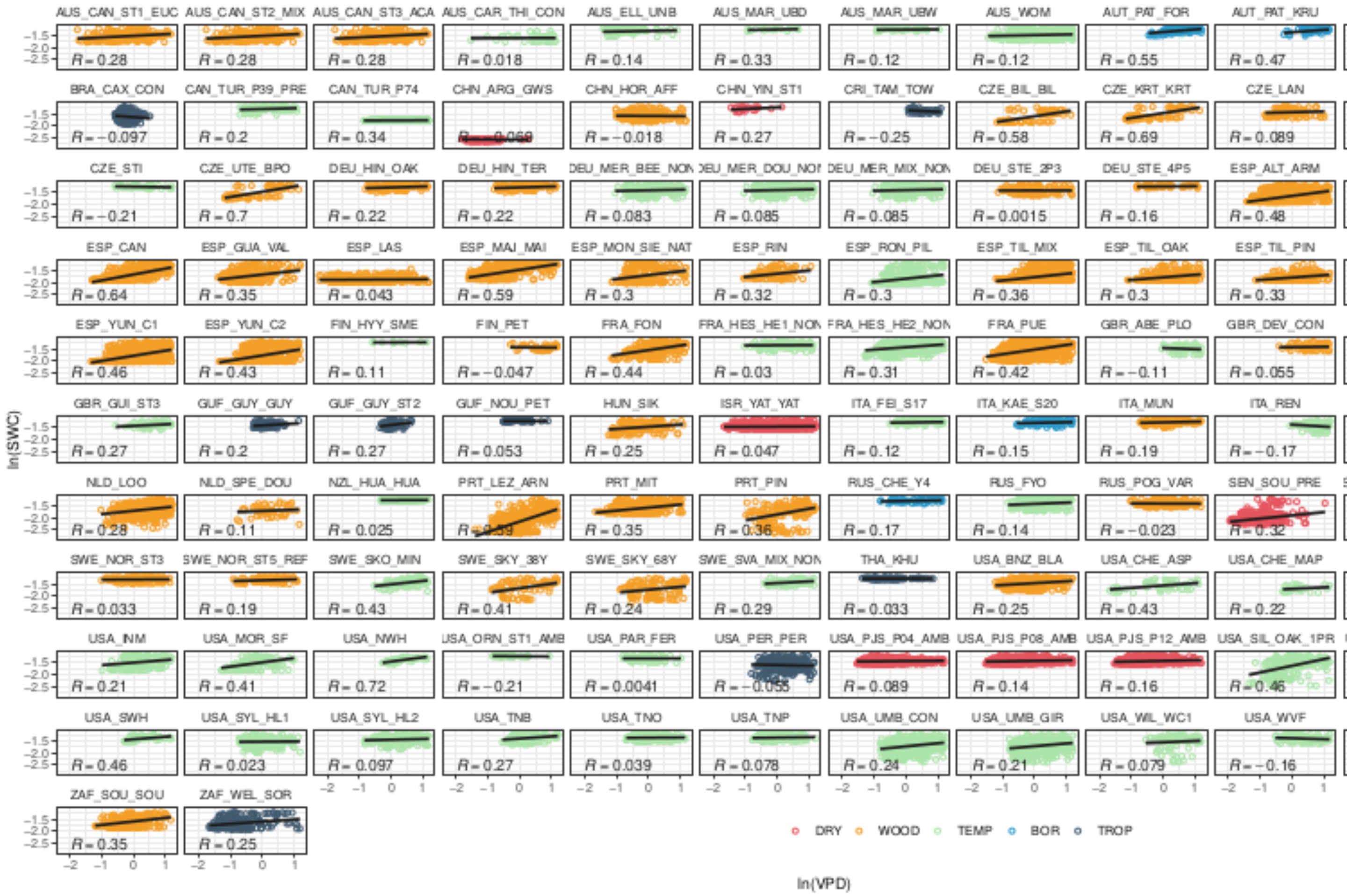

Figure S6: Correlations at the site level between VPD and SWC. R values are Pearson correlations. Different colors indica
and desert biomes; WOOD: woodlands and shrublands; TEMP: temperate biomes; BOR: boreal and tundra; TROP: tropica

Figure S7: Correlations at the site level between VPD and PPFD. R values are Pearson correlations. Different colors indica
and desert biomes; WOOD: woodlands and shrublands; TEMP: temperate biomes; BOR: boreal and tundra; TROP: tropical

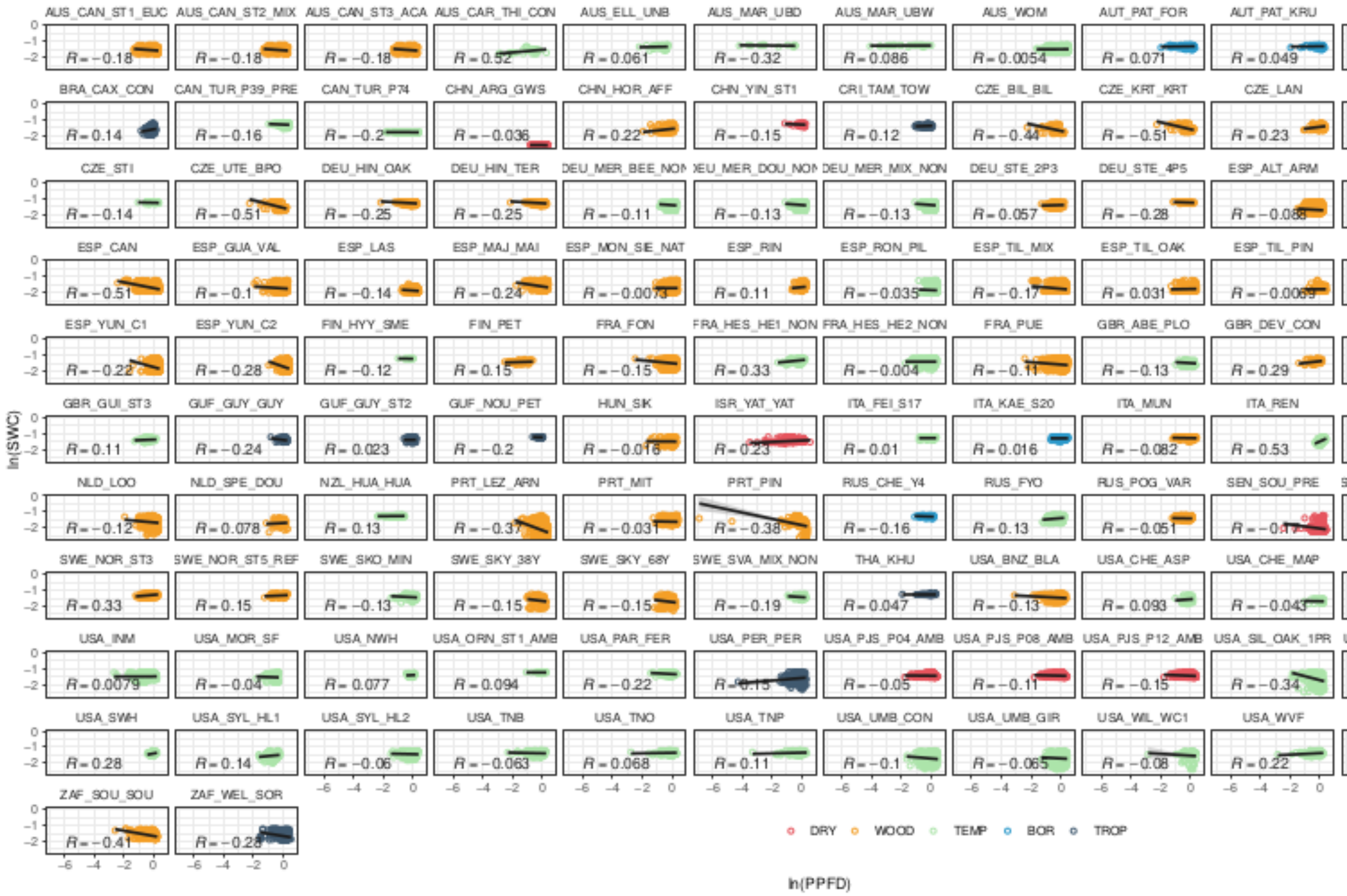

Figure S8: Correlations at the site level between PPFD and SWC. R values are Pearson correlations. Different colors indica
and desert biomes; WOOD: woodlands and shrublands; TEMP: temperate biomes; BOR: boreal and tundra; TROP: tropical

Table S1: SAPFLUXNET stand treatments included in the this study.

Plot treatment
NA
None
Control
control
Ambient Control
Control - Unthinned
natural conditions
Reference
1Premortality
2premortality
distructive sampling
Girdling early successional
Pre-thinning
Before thinning
Before Thinning
non thinned
none (periodict thinning every 5-6 years 20 to 25% of basal area)
Radiation Level
AMBIENT CO2 FACE rings
fertilization at plantation
AcaciaMonoculture
MixtureEucalyptusAndAcacia
EucalyptusMonoculture
Pre Irrigation

Table S2: SAPFLUXNET sites included in the study. Biome was estimated using a Whittaker diagram. *Indicates that the biome was manually adjusted and confirmed by SAPFLUXNET contributors.

Site code	Latitude	Longitude	Biome	# Tree-days	# Species	# Trees
AUS_CAN_ST1_EUC	-37.58	149.17	WOOD	500	1	12
AUS_CAN_ST2_MIX	-37.58	149.17	WOOD	1077	2	22
AUS_CAN_ST3_ACA	-37.58	149.17	WOOD	609	1	12
AUS_CAR_THI_CON	-38.38	146.68	TEMP	69	1	3
AUS_ELL_UNB	-36.78	146.58	TEMP	140	1	2
AUS_MAR_UBD	-37.69	145.56	TEMP	32	2	2
AUS_MAR_UBW	-37.89	145.57	TEMP	121	3	5
AUS_WOM	-37.42	144.09	TEMP	4454	2	11
AUT_PAT_FOR	47.21	11.45	BOR	286	1	3
AUT_PAT_KRU	47.21	11.45	BOR	105	1	2
AUT_PAT_TRE	47.21	11.45	BOR	133	1	3
BRA_CAM	-22.69	-45.52	TROP*	89	1	5
BRA_CAX_CON	-1.79	-51.43	TROP	2406	8	15
CAN_TUR_P39_PRE	42.71	-80.36	TEMP	2225	1	18
CAN_TUR_P74	42.71	-80.35	TEMP	10586	1	16
CHN_ARG_GWS	41.38	89.94	DRY	300	1	2
CHN_HOR_AFF	42.72	122.37	WOOD	2786	1	16
CHN_YIN_ST1	42.45	85.72	DRY	122	1	5
CRI_TAM_TOW	10.39	-84.63	TROP	1266	17	26
CZE_BIL_BIL	49.25	16.69	TEMP*	400	1	6
CZE_KRT_KRT	49.32	16.75	TEMP*	435	1	6
CZE_LAN	48.68	16.95	TEMP*	1775	3	17
CZE_RAJ_RAJ	49.44	16.70	TEMP*	360	1	6
CZE_SOB_SOB	49.25	16.69	TEMP*	1727	1	6
CZE_STI	49.04	17.97	TEMP	348	1	8
CZE_UTE_BPO	49.28	16.65	TEMP*	456	1	6
DEU_HIN_OAK	53.33	13.19	TEMP*	864	1	8
DEU_HIN_TER	53.33	13.19	TEMP*	1954	2	16
DEU_MER_BEE_NON	49.27	7.81	TEMP	841	1	8
DEU_MER_DOU_NON	49.27	7.81	TEMP	895	1	7
DEU_MER_MIX_NON	49.27	7.81	TEMP	1945	2	17
DEU_STE_2P3	53.10	13.00	TEMP*	1228	1	10
DEU_STE_4P5	53.10	13.00	TEMP*	402	1	10
ESP_ALT_ARM	40.78	-2.33	WOOD	8306	3	15
ESP_ALT_HUE	40.79	-2.29	WOOD	3698	2	8
ESP_ALT_TRI	40.80	-2.23	WOOD	5411	2	12
ESP_CAN	41.43	2.07	WOOD	6871	4	21
ESP_GUA_VAL	40.90	-4.03	WOOD	3424	1	24
ESP_LAS	28.31	-16.57	WOOD	4406	1	10
ESP_MAJ_MAI	39.94	-5.77	WOOD	2833	1	6
ESP_MON_SIE_NAT	41.12	-3.50	WOOD	2587	3	20
ESP_RIN	40.60	-6.02	WOOD	770	1	8
ESP_RON_PIL	36.69	-5.02	TEMP	4114	2	12
ESP_TIL_MIX	41.33	1.01	WOOD	15699	2	32
ESP_TIL_OAK	41.33	1.01	WOOD	2381	1	10
ESP_TIL_PIN	41.33	1.01	WOOD	1976	1	9
ESP_VAL_BAR	42.20	1.82	WOOD	1394	1	12
ESP_VAL_SOR	42.20	1.81	WOOD	1943	1	13
ESP_YUN_C1	36.72	-4.97	WOOD	2935	1	6
ESP_YUN_C2	36.72	-4.97	WOOD	830	1	6
FIN_HYY_SME	61.85	24.29	TEMP	10	1	1
FIN_PET	69.49	27.23	BOR*	216	1	7
FRA_FON	48.48	2.78	TEMP*	720	1	3
FRA_HES_HE1_NON	48.67	7.06	TEMP	1273	1	10
FRA_HES_HE2_NON	48.67	7.06	TEMP	4167	1	10
FRA_PUE	43.74	3.60	WOOD	23566	1	25
GBR_ABE_PLO	56.62	-3.80	TEMP	692	1	15
GBR_DEV_CON	56.03	-3.72	TEMP*	215	1	4
GBR_GUI_ST1	57.27	-4.82	TEMP	834	1	15

Table S2: SAPFLUXNET sites included in the study. Biome was estimated using a Whittaker diagram. *Indicates that the biome was manually adjusted and confirmed by SAPFLUXNET contributors. *(continued)*

Site code	Latitude	Longitude	Biome	# Tree-days	# Species	# Trees
GBR_GUI_ST2	57.27	-4.82	TEMP	621	1	9
GBR_GUI_ST3	57.27	-4.82	TEMP	444	1	8
GUF_GUY_GUY	5.28	-52.92	TROP	710	6	6
GUF_GUY_ST2	5.28	-52.91	TROP	885	7	11
GUF_NOU_PET	4.08	-52.68	TROP	923	10	22
HUN_SIK	47.93	20.44	WOOD	550	2	4
ISR_YAT_YAT	31.34	35.05	DRY	15766	1	24
ITA_FEI_S17	46.69	10.61	TEMP	378	1	6
ITA_KAE_S20	46.70	10.61	BOR	586	1	6
ITA_MUN	46.68	10.58	TEMP*	885	1	6
ITA_REN	46.59	11.43	TEMP	577	3	8
ITA_RUN_N20	46.70	10.64	BOR	766	2	8
MEX_COR_YP	19.49	-97.04	TEMP	113	1	7
NLD_LOO	52.17	5.74	TEMP*	3033	1	6
NLD_SPE_DOU	52.25	5.69	TEMP*	150	1	3
NZL_HUA_HUA	-36.80	174.49	TEMP	1107	1	6
PRT_LEZ_ARN	38.83	-8.82	WOOD	1764	1	4
PRT_MIT	38.54	-8.00	WOOD	1510	1	4
PRT_PIN	38.25	-8.76	WOOD	2991	2	20
RUS_CHE_Y4	68.74	161.41	BOR	587	1	11
RUS_FYO	56.46	32.92	TEMP	2338	3	17
RUS_POG_VAR	56.36	92.95	TEMP*	1290	3	9
SEN_SOU_PRE	16.34	-15.43	DRY	1706	1	3
SWE_NOR_ST1_BEF	60.09	17.48	TEMP*	843	2	22
SWE_NOR_ST2	60.09	17.48	TEMP*	194	2	6
SWE_NOR_ST3	60.09	17.48	TEMP*	1195	2	37
SWE_NOR_ST5_REF	60.08	17.48	TEMP*	1255	3	25
SWE_SKO_MIN	58.36	12.15	TEMP	1072	1	11
SWE_SKY_38Y	60.13	17.84	TEMP*	455	1	12
SWE_SKY_68Y	60.10	17.83	TEMP*	1046	2	12
SWE_SVA_MIX_NON	64.26	19.77	TEMP	1549	2	20
THA_KHU	15.27	103.08	TROP	1278	1	6
USA_BNZ_BLA	64.70	-148.32	BOR*	1705	1	6
USA_CHE_ASP	45.94	-90.27	TEMP	3995	6	142
USA_CHE_MAP	45.95	-90.26	TEMP	3378	2	145
USA_DUK_HAR	36.98	-79.09	TEMP	621	6	33
USA_HIL_HF2	36.22	-78.86	TEMP	263	5	22
USA_INM	39.32	-86.41	TEMP	1648	6	9
USA_MOR_SF	39.32	-86.41	TEMP	680	4	6
USA_NWH	34.58	-91.26	TEMP	525	2	10
USA_ORN_ST1_AMB	35.90	-84.33	TEMP	310	1	8
USA_PAR_FER	35.80	-76.67	TEMP	736	1	8
USA_PER_PER	30.21	-83.87	TROP	18180	1	80
USA_PJS_P04_AMB	34.39	-106.53	DRY	12129	2	10
USA_PJS_P08_AMB	34.39	-106.53	DRY	10754	2	10
USA_PJS_P12_AMB	34.39	-106.53	DRY	12528	2	10
USA_SIL_OAK_1PR	39.92	-74.60	TEMP	2304	4	18
USA_SIL_OAK_2PR	39.92	-74.60	TEMP	6790	4	22
USA_SMI_SER	38.89	-76.56	TEMP*	1733	5	30
USA_SWH	34.11	-91.13	TEMP	956	2	16
USA_SYL_HL1	46.24	-89.35	TEMP	8620	3	48
USA_SYL_HL2	46.24	-89.35	TEMP	3678	4	20
USA_TNB	36.47	-84.70	TEMP	1240	4	8
USA_TNO	35.97	-84.28	TEMP	1271	5	9
USA_TNP	35.96	-84.29	TEMP	1342	5	9
USA_UMB_CON	45.56	-84.71	TEMP	17923	5	57
USA_UMB_GIR	45.56	-84.70	TEMP	19175	4	57
USA_WIL_WC1	45.81	-90.09	TEMP	1306	5	16
USA_WVF	39.06	-79.69	TEMP	989	5	8

Table S2: SAPFLUXNET sites included in the study. Biome was estimated using a Whittaker diagram. *Indicates that the biome was manually adjusted and confirmed by SAPFLUXNET contributors. *(continued)*

Site code	Latitude	Longitude	Biome	# Tree-days	# Species	# Trees
ZAF_FRA_FRA	-33.88	19.06	WOOD	563	1	3
ZAF_RAD	-34.08	19.11	WOOD	660	1	3
ZAF_SOU_SOU	-34.09	19.09	WOOD	424	1	2
ZAF_WEL_SOR	-33.48	18.96	WOOD*	538	1	3

Table S3: Table of equivalence between Whittaker biomes and the groups of biomes used in the study.

Original biome name	Study biome group
Desert	DRY
Temperate grassland desert	DRY
Subtropical desert	DRY
Woodland/shrubland	WOOD
Temperate forest	TEMP
Boreal forest	BOR
Tundra	BOR
Tropical rainforest	TROP
Tropical seasonal forest/savanna	TROP

Table S4: Summary table of site level R^2_{VPD}, R^2_{SWC}, R^2_{PPFD}, climate, soil properties and vegetation structure data. PPET is in [mm mm^{-1}], P-PET$_{sd}$ is in [mm], Clay and Sand are in [%], Total N is in [g kg^{-1}], Stand height is in [m], LAI is in [m$^2_{leaves}$ m$^2_{soil}$]. Letters show data source: a = SAPFLUXNET, b = Global rasters, c = SAPFLUXNET plant height.

Site code	R^2_{VPD}	R^2_{SWC}	R^2_{PPFD}	RelImp VPD	RelImp SWC	RelImp PPFD	PPET	$P-PET_{sd}$	Clay	Sand	Total N	Bedro
AUS_CAN_ST1_EUC	0.77	0.49	0.60	0.66	0.34	0.00	1.23	47.52	26.30 b	45.10 b	1.02	184
AUS_CAN_ST2_MIX	0.83	0.62	0.72	0.83	0.17	0.00	1.23	47.52	26.30 b	45.10 b	1.02	184
AUS_CAN_ST3_ACA	0.83	0.69	0.75	0.84	0.15	0.02	1.23	47.52	26.30 b	45.10 b	1.02	184
AUS_CAR_THI_CON	0.41	0.00	0.07	0.81	0.05	0.14	1.36	49.01	27.20 b	44.30 b	2.34	111
AUS_ELL_UNB	0.86	0.46	0.76	0.98	0.00	0.02	1.08	67.16	26.70 b	48.50 b	1.95	63
AUS_MAR_UBD	0.81	0.23	0.37	0.82	0.15	0.04	1.35	70.37	26.60 b	44.60 b	1.90	89
AUS_MAR_UBW	0.90	0.78	0.81	0.89	0.00	0.11	1.21	65.38	27.90 b	43.90 b	2.00	173
AUS_WOM	0.79	0.52	0.51	0.79	0.00	0.20	1.09	69.35	25.90 b	52.90 b	1.97	172
AUT_PAT_FOR	0.77	0.69	0.64	0.94	0.00	0.06	2.17	16.78	5.00 a	60.00 a	3.94	180
AUT_PAT_KRU	0.43	0.27	0.28	0.84	0.07	0.09	2.17	16.78	5.00 a	60.00 a	3.94	180
AUT_PAT_TRE	0.56	0.27	0.20	0.70	0.30	0.00	2.17	16.78	5.00 a	60.00 a	3.94	180
BRA_CAM	0.84	0.70	0.70	0.65	0.27	0.07	1.66	88.82	27.60 b	52.00 b	2.26	200
BRA_CAX_CON	0.75	0.68	0.68	0.73	0.00	0.27	1.90	122.90	8.00 a	79.00 a	1.45	197
CAN_TUR_P39_PRE	0.49	0.33	0.31	0.72	0.09	0.19	1.39	42.08	1.00 a	98.00 a	1.58	200
CAN_TUR_P74	0.21	0.32	0.16	0.31	0.33	0.35	1.39	41.87	1.00 a	98.00 a	1.60	200
CHN_ARG_GWS	0.45	0.34	0.35	0.52	0.45	0.03	0.01	63.51	17.70 b	46.00 b	0.70	172
CHN_HOR_AFF	0.37	0.33	0.32	0.51	0.47	0.01	0.59	31.24	8.00 a	83.00 a	1.00	200
CHN_YIN_ST1	0.46	0.46	0.44	0.48	0.41	0.11	0.19	35.09	20.80 b	32.90 b	2.41	148
CRI_TAM_TOW	0.68	0.68	0.67	0.47	0.15	0.37	3.57	159.99	36.10 b	34.70 b	2.75	200
CZE_BIL_BIL	0.53	0.53	0.41	0.52	0.20	0.29	0.71	28.98	29.60 b	27.40 b	1.91	200
CZE_KRT_KRT	0.61	0.50	0.30	0.62	0.04	0.34	0.85	27.00	26.00 b	27.40 b	2.10	200
CZE_LAN	0.74	0.73	0.69	0.67	0.07	0.26	0.66	37.49	17.80 a	71.80 a	2.46	200
CZE_RAJ_RAJ	0.35	0.36	0.39	0.37	0.03	0.60	0.99	26.14	21.80 b	33.90 b	1.96	200
CZE_SOB_SOB	0.40	0.43	0.13	0.49	0.30	0.21	0.71	28.98	29.60 b	27.40 b	1.91	200
CZE_STI	0.52	0.36	0.43	0.69	0.23	0.09	1.13	27.10	34.20 a	47.60 a	1.65	200
CZE_UTE_BPO	0.64	0.67	0.53	0.41	0.17	0.42	0.75	29.86	26.70 b	23.80 b	2.71	200
DEU_HIN_OAK	0.36	0.18	0.29	0.93	0.06	0.01	0.95	35.10	17.90 b	49.90 b	2.42	200
DEU_HIN_TER	0.22	0.17	0.18	0.74	0.02	0.24	0.95	35.10	18.00 b	50.50 b	2.05	200
DEU_MER_BEE_NON	0.38	0.25	0.27	0.80	0.05	0.15	1.48	47.33	4.00 a	71.00 a	2.56	200
DEU_MER_DOU_NON	0.38	0.25	0.18	0.58	0.29	0.14	1.48	47.33	4.00 a	71.00 a	2.56	200
DEU_MER_MIX_NON	0.35	0.21	0.25	0.85	0.01	0.14	1.48	47.33	4.00 a	71.00 a	2.56	200
DEU_STE_2P3	0.48	0.14	0.25	0.84	0.08	0.08	0.90	37.45	2.50 a	92.50 a	3.28	200
DEU_STE_4P5	0.45	0.28	0.33	0.64	0.32	0.04	0.90	37.45	2.50 a	92.50 a	3.28	200
ESP_ALT_ARM	0.44	0.39	0.29	0.77	0.19	0.04	0.66	65.80	21.90 b	41.50 b	1.27	187
ESP_ALT_HUE	0.42	0.27	0.22	0.77	0.00	0.23	0.51	63.08	21.60 b	35.90 b	1.46	200
ESP_ALT_TRI	0.48	0.42	0.26	0.67	0.21	0.13	0.57	63.48	21.00 b	40.00 b	1.31	196
ESP_CAN	0.51	0.44	0.35	0.62	0.09	0.28	0.94	46.91	32.90 b	28.30 b	1.76	179
ESP_GUA_VAL	0.50	0.30	0.25	0.71	0.00	0.29	0.68	69.09	24.80 b	40.90 b	1.27	200
ESP_LAS	0.24	0.26	0.07	0.43	0.45	0.13	1.63	37.89	1.00 a	70.00 a	1.65	197
ESP_MAJ_MAI	0.53	0.47	0.28	0.69	0.15	0.16	0.76	97.45	9.00 a	80.00 a	1.18	200
ESP_MON_SIE_NAT	0.38	0.33	0.40	0.49	0.05	0.45	0.62	63.05	20.80 b	41.90 b	1.45	200
ESP_RIN	0.82	0.61	0.60	0.96	0.00	0.04	0.85	76.30	15.00 a	9.00 a	2.17	200
ESP_RON_PIL	0.34	0.26	0.16	0.59	0.11	0.31	1.05	93.66	18.00 a	30.00 a	1.86	200
ESP_TIL_MIX	0.40	0.42	0.30	0.43	0.17	0.40	0.77	48.10	20.00 a	60.00 a	1.44	162
ESP_TIL_OAK	0.16	0.37	0.18	0.29	0.35	0.37	0.77	48.10	20.00 a	60.00 a	1.44	162
ESP_TIL_PIN	0.20	0.39	0.06	0.28	0.55	0.17	0.79	48.10	20.00 a	60.00 a	1.78	188

Table S4: Summary table of site level R^2_{VPD}, R^2_{SWC}, R^2_{PPFD}, climate, soil properties and vegetation structure data. PPET is in [mm mm^{-1}], P-PET$_{sd}$ is in [mm], Clay and Sand are in [%], Total N is in [g kg^{-1}], Stand height is in [m], LAI is in [m$^2_{leaves}$ m$^2_{soil}$]. Letters show data source: a = SAPFLUXNET, b = Global rasters, c = SAPFLUXNET plant height. *(continued)*

Site code	R^2_{VPD}	R^2_{SWC}	R^2_{PPFD}	RelImp VPD	RelImp SWC	RelImp PPFD	PPET	$P-PET_{sd}$	Clay	Sand	Total N	Bedro
ESP_VAL_BAR	0.56	0.24	0.27	0.87	0.00	0.13	0.70	34.07	32.63 a	9.81 a	1.94	200
ESP_VAL_SOR	0.50	0.32	0.26	0.66	0.10	0.24	0.78	32.15	20.00 a	60.00 a	2.04	200
ESP_YUN_C1	0.29	0.44	0.17	0.17	0.67	0.16	0.83	93.65	29.00 a	22.00 a	1.37	197
ESP_YUN_C2	0.27	0.61	0.24	0.22	0.43	0.35	0.78	91.33	29.00 a	22.00 a	1.37	188
FIN_HYY_SME	0.51	0.01	0.10	0.61	0.10	0.29	1.20	38.32	6.50 a	37.00 a	1.67	200
FIN_PET	0.63	0.63	0.58	0.40	0.60	0.01	1.13	26.34	7.30 b	60.80 b	5.08	200
FRA_FON	0.68	0.62	0.64	0.72	0.22	0.06	0.89	45.10	19.00 a	37.00 a	1.26	200
FRA_HES_HE1_NON	0.42	0.53	0.43	0.41	0.26	0.33	1.31	47.72	25.00 a	8.00 a	1.41	200
FRA_HES_HE2_NON	0.25	0.35	0.12	0.45	0.27	0.28	1.31	47.72	25.00 a	8.00 a	1.41	200
FRA_PUE	0.40	0.47	0.27	0.46	0.27	0.27	1.27	70.16	39.00 a	26.00 a	1.69	195
GBR_ABE_PLO	0.28	0.26	0.21	0.51	0.23	0.25	1.92	47.48	10.00 a	60.00 a	3.70	179
GBR_DEV_CON	0.88	0.48	0.62	0.93	0.04	0.04	1.43	44.38	14.80 b	56.90 b	3.44	200
GBR_GUI_ST1	0.80	0.78	0.77	0.58	0.01	0.41	3.19	68.11	3.70 b	80.40 b	14.26	197
GBR_GUI_ST2	0.59	0.55	0.47	0.59	0.06	0.35	3.19	68.11	3.70 b	80.40 b	14.26	197
GBR_GUI_ST3	0.82	0.81	0.77	0.66	0.03	0.31	3.19	68.11	3.70 b	80.40 b	14.26	197
GUF_GUY_GUY	0.96	0.90	0.93	0.82	0.07	0.11	2.88	135.18	43.00 a	48.00 a	1.53	200
GUF_GUY_ST2	0.79	0.78	0.75	0.46	0.49	0.04	3.02	141.34	43.20 a	47.80 a	1.66	200
GUF_NOU_PET	0.81	0.55	0.71	1.00	0.00	0.00	2.69	158.16	59.20 a	33.20 a	2.22	200
HUN_SIK	0.79	0.36	0.48	0.93	0.01	0.06	0.70	39.64	30.40 b	44.00 b	1.64	200
ISR_YAT_YAT	0.28	0.32	0.14	0.43	0.57	0.00	0.28	83.43	28.00 a	31.00 a	0.71	178
ITA_FEI_S17	0.54	0.39	0.30	0.68	0.13	0.19	1.08	22.97	8.00 a	76.00 a	3.11	117
ITA_KAE_S20	0.62	0.47	0.47	0.72	0.06	0.22	1.24	22.97	17.00 a	50.00 a	3.64	121
ITA_MUN	0.56	0.39	0.42	0.74	0.22	0.04	0.80	29.87	7.00 a	55.00 a	1.93	188
ITA_REN	0.79	0.73	0.74	0.99	0.00	0.01	1.61	12.59	17.70 b	47.90 b	2.73	143
ITA_RUN_N20	0.78	0.71	0.71	0.88	0.00	0.12	1.39	15.28	14.00 a	54.00 a	3.33	123
MEX_COR_YP	0.68	0.23	0.31	0.79	0.05	0.16	1.42	81.77	22.20 b	46.40 b	2.94	200
NLD_LOO	0.18	0.12	0.12	0.79	0.00	0.21	1.33	41.67	1.00 a	99.00 a	2.61	200
NLD_SPE_DOU	0.75	0.59	0.63	0.85	0.03	0.12	1.42	39.80	4.80 b	80.70 b	1.62	200
NZL_HUA_HUA	0.65	0.61	0.59	0.70	0.15	0.15	2.62	42.52	71.20 a	13.20 a	1.73	200
PRT_LEZ_ARN	0.59	0.28	0.27	0.78	0.01	0.21	0.72	77.42	5.04 a	90.38 a	1.52	200
PRT_MIT	0.66	0.55	0.32	0.61	0.33	0.06	0.51	80.80	16.10 b	64.50 b	1.33	200
PRT_PIN	0.65	0.55	0.38	0.65	0.32	0.02	0.76	74.76	16.60 b	61.20 b	1.26	200
RUS_CHE_Y4	0.32	0.22	0.24	0.94	0.00	0.06	0.62	34.23	21.10 b	23.20 b	4.96	200
RUS_FYO	0.61	0.56	0.54	0.81	0.02	0.17	1.24	30.87	18.20 b	48.80 b	3.77	198
RUS_POG_VAR	0.70	0.50	0.58	0.81	0.00	0.19	0.70	33.02	28.60 b	37.50 b	2.64	200
SEN_SOU_PRE	0.64	0.40	0.22	0.66	0.34	0.01	0.13	43.94	6.00 a	90.00 a	0.23	200
SWE_NOR_ST1_BEF	0.74	0.65	0.64	0.61	0.28	0.10	1.07	36.70	5.80 a	58.60 a	2.63	185
SWE_NOR_ST2	0.32	0.29	0.23	0.55	0.02	0.44	1.07	36.70	5.80 a	58.60 a	2.63	185
SWE_NOR_ST3	0.55	0.59	0.56	0.48	0.22	0.30	1.07	36.70	5.80 a	58.60 a	2.63	185
SWE_NOR_ST5_REF	0.53	0.56	0.53	0.48	0.20	0.32	1.07	36.55	19.20 b	43.50 b	2.83	190
SWE_SKO_MIN	0.71	0.70	0.67	0.52	0.04	0.44	1.60	45.86	17.30 b	52.00 b	2.48	133
SWE_SKY_38Y	0.34	0.43	0.37	0.05	0.94	0.00	1.39	33.61	21.70 b	43.80 b	3.93	184
SWE_SKY_68Y	0.35	0.53	0.34	0.05	0.83	0.11	1.30	33.80	18.90 b	46.50 b	4.15	184
SWE_SVA_MIX_NON	0.65	0.54	0.57	0.78	0.22	0.00	1.33	34.34	0.50 a	92.50 a	1.67	200
THA_KHU	0.50	0.41	0.41	0.78	0.21	0.01	0.83	84.24	10.00 a	65.00 a	0.75	200
USA_BNZ_BLA	0.52	0.37	0.46	0.68	0.21	0.10	0.69	33.86	10.30 b	36.80 b	2.57	200
USA_CHE_ASP	0.67	0.32	0.30	0.91	0.03	0.06	1.23	20.06	12.00 a	74.00 a	1.52	200

Table S4: Summary table of site level R^2_{VPD}, R^2_{SWC}, R^2_{PPFD}, climate, soil properties and vegetation structure data. PPET is in [mm mm^{-1}], P-PET$_{sd}$ is in [mm], Clay and Sand are in [%], Total N is in [g kg^{-1}], Stand height is in [m], LAI is in [m^2_{leaves} m^2_{soil}]. Letters show data source: a = SAPFLUXNET, b = Global rasters, c = SAPFLUXNET plant height. *(continued)*

Site code	R^2_{VPD}	R^2_{SWC}	R^2_{PPFD}	RelImp VPD	RelImp SWC	RelImp PPFD	PPET	$P-PET_{sd}$	Clay	Sand	Total N	Bedro
USA_CHE_MAP	0.57	0.52	0.52	0.76	0.06	0.18	1.22	19.85	6.63 a	59.31 a	2.54	200
USA_DUK_HAR	0.72	0.62	0.67	0.91	0.02	0.07	1.12	41.33	33.90 b	31.00 b	0.76	200
USA_HIL_HF2	0.75	0.71	0.74	0.61	0.00	0.39	1.14	37.46	26.00 a	43.00 a	0.71	200
USA_INM	0.40	0.35	0.38	0.56	0.00	0.44	1.18	39.20	26.70 b	8.00 b	1.05	200
USA_MOR_SF	0.65	0.58	0.49	0.90	0.09	0.01	1.18	39.20	30.00 a	10.00 a	1.05	200
USA_NWH	0.88	0.85	0.73	0.80	0.04	0.15	1.05	59.56	36.70 b	4.90 b	0.80	200
USA_ORN_ST1_AMB	0.63	0.62	0.53	0.51	0.10	0.39	1.14	61.36	24.00 a	21.00 a	0.85	200
USA_PAR_FER	0.43	0.17	0.22	0.69	0.04	0.27	1.32	25.96	10.00 a	60.00 a	1.75	200
USA_PER_PER	0.55	0.30	0.37	0.85	0.01	0.14	1.32	34.41	3.40 b	89.20 b	6.13	200
USA_PJS_P04_AMB	0.31	0.09	0.26	0.74	0.03	0.23	0.25	49.32	6.00 a	52.00 a	0.82	186
USA_PJS_P08_AMB	0.33	0.10	0.22	0.94	0.03	0.03	0.25	49.32	3.00 a	49.00 a	0.82	186
USA_PJS_P12_AMB	0.28	0.14	0.15	0.63	0.37	0.00	0.25	49.32	6.00 a	54.00 a	0.82	186
USA_SIL_OAK_1PR	0.38	0.40	0.36	0.29	0.58	0.13	1.36	38.70	1.00 a	98.00 a	0.74	200
USA_SIL_OAK_2PR	0.39	0.32	0.36	0.92	0.06	0.01	1.36	38.70	1.00 a	98.00 a	0.74	200
USA_SMI_SER	0.51	0.37	0.37	0.67	0.32	0.01	1.03	40.05	28.70 b	30.90 b	0.82	200
USA_SWH	0.86	0.63	0.50	0.94	0.01	0.05	1.09	62.29	43.10 b	6.30 b	0.69	200
USA_SYL_HL1	0.46	0.36	0.38	0.97	0.03	0.00	1.27	25.01	8.90 b	51.00 b	1.41	200
USA_SYL_HL2	0.47	0.46	0.46	0.55	0.01	0.44	1.27	25.01	8.90 b	51.00 b	1.41	200
USA_TNB	0.25	0.27	0.24	0.41	0.12	0.46	1.39	48.33	21.60 b	34.90 b	0.84	200
USA_TNO	0.40	0.40	0.38	0.50	0.22	0.28	1.41	60.02	29.60 b	30.20 b	0.83	200
USA_TNP	0.33	0.36	0.31	0.40	0.37	0.23	1.41	61.60	31.60 b	26.60 b	0.81	200
USA_UMB_CON	0.51	0.39	0.38	0.79	0.03	0.18	1.30	30.60	1.00 a	92.00 a	2.02	200
USA_UMB_GIR	0.43	0.35	0.34	0.78	0.05	0.17	1.25	30.69	1.00 a	92.00 a	2.49	200
USA_WIL_WC1	0.33	0.18	0.16	0.82	0.16	0.02	1.19	20.23	6.90 b	53.20 b	1.01	200
USA_WVF	0.28	0.26	0.25	0.59	0.06	0.36	1.63	30.35	24.90 b	29.90 b	1.37	200
ZAF_FRA_FRA	0.43	0.08	0.14	0.92	0.00	0.08	0.90	99.17	20.00 b	69.90 b	0.95	200
ZAF_RAD	0.46	0.42	0.40	0.57	0.10	0.33	0.95	82.73	21.30 b	61.40 b	1.18	200
ZAF_SOU_SOU	0.39	0.22	0.21	0.59	0.06	0.35	0.97	86.39	23.00 b	61.90 b	1.13	200
ZAF_WEL_SOR	0.62	0.33	0.34	0.63	0.08	0.29	0.50	79.71	20.00 a	60.00 a	0.81	179